Cluster Production in $^{197}Au + ^{197}Au$ Collisions at 11.6 A·GeV/c

by

SHELDON J. PARK
B.A. University of California, Berkeley (1991)

Submitted to the Department of Physics
in partial fulfillment of the requirements for the degree of
Master of Science in Physics

at the

Massachusetts Institute of Technology
January 14, 1994

Signature of Author _____
Department of Physics
January, 1994

Certified by _____
Stephen G. Steadman
Department of Physics
Thesis Supervisor

Accepted by _____
George F. Koster
Chairman, Physics Graduate Committee

Cluster Production in $^{197}Au + ^{197}Au$ Collisions at 11.6 A·GeV/c

by

SHELDON J. PARK

Submitted to the Department of Physics
in partial fulfillment of the requirements for the degree of
Master of Science in Physics

Abstract

The invariant differential cross sections for p, d, t, and ^{3}He produced in central, peripheral, and minimum-bias events from $^{197}Au+^{197}Au$ collisions at 11.6 A·GeV/c are measured. Their integrated yields and the fitted inverse slopes (temperatures) are derived. The deuteron temperatures are shown to be larger than the proton temperatures in central collisions, but whether the tritons have larger temperatures than the deuterons is inconclusive. Evidence for the collective transverse expansion of the source is lacking.

Cluster production at the AGS energy at central rapidity is qualitatively described by the coalescence model, and the deuteron rapidity distribution (dN/dy) in particular is consistent with this picture, whereas the heavy clusters have significant contributions from the fragmentation of the spectator matter.

A method of measuring the source size by using the deuteron integrated yields without assuming thermal equilibrium for the source is presented. The technique is developed in the framework of the well-known Second Order Interferometry of identical particles. It is predicted that the strong interaction between the proton and the neutron affects their relative momentum distribution and thereby influences the deuteron dN/dy. The uncertainties in the upper relative momentum cut and the upper spatial cut for coalescence do not allow a precise measurement of the source size. The dynamical correlation between the momentum and spatial variables has been estimated based on the crude approximation of the particles being emitted preferentially perpendicular to the source surface, and was put in by hand in the prediction for the deuteron dN/dy. The source size is extracted by comparing the measured deuteron dN/dy with the predictions for various source sizes. In this way, the RMS of the source is estimated to be ~10 fm for a coalescence momentum cut of 60 MeV/c. The difference between the proton and the deuteron temperatures is not resolved by introducing the low-q enhancement.

Thesis Supervisor: Dr. Stephen G. Steadman
Title: Senior Research Scientist in Physics

Contents

List of Figures

Chapter 1

Introduction

The standard approach to understand deuteron production in high energy nuclear collisions is to assume that the deuteron momentum distribution is proportional to the product of the proton momentum distribution and the neutron momentum distribution. This is a purely statistical approach, based on the reasoning that the deuteron density in momentum space should be proportional to the probability of finding a neutron within a small sphere of radius p_0 around the proton momentum. But because the argument is intuitive and plausible, it has found application in a variety of models for cluster production.

The usefulness of the parameter p_0 measured from the momentum distributions of the nuclear clusters lies in its relationship to the size of the volume in which thermal equilibrium has been reached. While this gives a strong incentive to study the deuteron yield carefully, one needs to make the assumption of thermalization within the volume in order to deduce its size. The source size is an important parameter to measure because it is a direct indicator of the baryon density in the collision region. Since there is as yet no experimental evidence that thermal equilibrium has been achieved, it is desirable to be able to measure the source size without such an assumption. First, the nuclear collision is simulated using a phenomenological model to obtain the particle distributions in the absence of the interactions responsible for cluster formation. The simulated output is modified by applying the nucleon-nucleon momentum correlation. The deuteron yields can be predicted based on the modified distribution, subject to the coalescence momentum and spatial cuts, to be

determined from the deuteron wave function, which are then compared with the data. By varying the amount of the momentum correlation, different deuteron yields are predicted. As will be shown, the amount of the correlation depends on the size of the volume emitting the nucleons, irrespective of its thermal status, thereby connecting the deuteron yields to the source size.

In the next section, a few models for cluster production based on coalescence in phase space are reviewed to introduce the concept more precisely. The concept of coalescence is important to the analysis presented here, for coalescence in phase space is necessary to produce deuterons from the single particle distributions. These models serve as an example of how the idea of coalescence is currently being used to explain cluster formation. The review also summarizes the steps involved in getting the source size from the deuteron rapidity distribution, dN/dy, in these models.

1.1 Models for Cluster Production

Coalescence Model

The essence of the Coalescence Model can be summarized in one equation [Sar89]:

$$\gamma \frac{d^3N_A}{dP_A^3} = \frac{2s_A+1}{2^A}\frac{1}{N!Z!}\left(\frac{4\pi}{3}p_0^3\right)^{A-1}\left(\gamma\frac{d^3N_n}{dp_n^3}\right)^N\left(\gamma\frac{d^3N_p}{dp_p^3}\right)^Z \tag{1.1}$$

for a cluster of N neutrons, Z protons. A=N+Z, $\gamma = \frac{p}{E}$ is the usual Lorentz contraction factor, s_A is the spin of the cluster in the ground state, and p_0 is a parameter to be determined experimentally from Eq. (1.1). p_0 physically corresponds to the maximum momentum difference a nucleon-nucleon pair can have and still form a bound state. In this form the equation does not account for any nuclear medium effect which may influence cluster formation. Also the equation is correct only to first order because the proton and neutron distributions used on the right hand side are final state distributions, i.e. after some protons and neutrons have already coalesced to clusters, and hence differ from the proton and neutron distributions prior to coalescence. Though there is no *a priori* correct value for p_0, one may expect it to

be related to the binding energy of the cluster in some way. In practice p_0 remains the only unknown in the equation. Its value measured by [Sar89] for central ^{28}Si+^{197}Au collisions at 14.6 A·GeV/c is about 60-70MeV/c and for p+A collisions it is around 140-180MeV/c.

There is a possibility that p_0 may be momentum dependent. When this happens, the model contains too many fitting parameters and therefore loses predictive power. Momentum dependence can arise if the transverse momentum distributions of the deuterons and the protons, which are approximately exponential in $m_t = \sqrt{p_t^2 + m_0^2}$, are described by two different inverse slopes. Then the ratio R of the deuteron cross-section to the proton cross-section squared becomes a function of p_t; and hence p_0 becomes a function of p_t. In the collision system studied for this thesis, ^{197}Au+^{197}Au at 11.6 A·GeV/c, the deuterons have a larger inverse slope than the protons. Therefore, the coalescence model with a constant p_0 is not entirely valid for our system. This difficulty, in practice, is avoided by taking an average $< R >_{p_t}$ before extracting p_0. Also, the model never makes a cut in coordinate space similar to the momentum cut, so the values from [Sar89] are probably lower limits. We should expect them to become larger, when the coordinate space cut is also included.

Sudden Approximation [Cse86]

In the Coalescence Model, different p_0's are obtained for different clusters, and since the model does not offer interpretation of these p_0's beyond the qualitative description given above, it has only limited usefulness in explaining cluster production. The Sudden Approximation Model improves on the Coalescence Model by making three assumptions: 1. Condensation of independent nucleons into nuclear clusters takes place on a time scale shorter than the interparticle collision rate. 2. The nucleon distribution is uniform over the spatial extent of the cluster. 3. The nucleon phase space distribution is independent of position within some volume V. The first two assumptions allow one to write the wave function of the cluster as a product of the wave functions of the constituent nucleons, while the last assumption—which implies that thermalization has been achieved throughout the source—relates their wave functions to the source volume and the differential cross sections. This

leads to an independent equation containing the volume V as a parameter rather than the coalescence radius p_0:

$$\frac{d^3N_A}{dP_A^3} = \frac{2s_A+1}{2^A}\left[\frac{(2\pi)^3}{V}\right]^{A-1}\left(\frac{d^3N_n}{dp_n^3}\right)^N\left(\frac{d^3N_p}{dp_p^3}\right)^Z. \tag{1.2}$$

Comparing Eqs. 1.1 and 1.2, a formula can be derived to relate the fitting parameter p_0 to the source volume:

$$\left(\frac{1}{N!Z!}\right)^{1/(A-1)}\gamma\frac{4\pi}{3}p_0^3 \longleftrightarrow \frac{(2\pi)^3}{V}. \tag{1.3}$$

In other words, the Coalescence Model plus the assumption of thermal equilibrium gives an estimate of the effective interaction volume at the time of cluster formation. As in the Coalescence Model, p_0 is the p_t-averaged value of $p_0(p_t)$.

Thermodynamic Model [Mek77]

If one further assumes chemical equilibrium among protons, neutrons and light nuclei, then the system possesses all the features of thermodynamic equilibrium, and can be studied using statistical mechanics. For instance, all phase space points are populated according to the Boltzmann factor associated with them, and the ratios of the yields of various clusters are determined by the nucleon chemical potential. The particle momentum distribution is then an exponential of the particle's kinetic energy in the rest frame of the emitting system, giving it a characteristic Boltzmann p_t distribution with temperature T_0. Since chemical equilibrium is believed to proceed at a slower pace than thermal equilibrium, the thermodynamic equilibrium would take longer than thermalization alone, but if achieved the particle spectra can be explained with one parameter T_0.

Fragmentation

One model for cluster production that is not based on the idea of coalescence is the Fragmentation Model. This process is particularly relevant to the production of heavy clusters (t,^{3}He...). At a given impact parameter, parts of the original nuclei are in the direct path of each other and therefore "participate" in the collision. The remaining parts of the nuclei, even though they are only spectators, become unstable and can emit clusters through frag-

mentation. These clusters have much smaller average kinetic energy than the ones created through coalescence, and their production is centered around the target (and projectile) rapidities, so one can recognize the fragmentation component by its small inverse slope in the p_t spectrum and the peak in dN/dy around $y = 0$.

1.2 Thesis Objective

In relativistic heavy ion collisions, a large number of nucleons, clusters of light nuclei, and pions inhabit the interaction region, and it is thought that statistical considerations play a more fundamental role in deciding the final state than any particular dynamic interaction [Mek78]. Yet, even in a system where thermodynamic equilibrium has been achieved, there is a pronounced correlation at low relative momentum between two protons. A similar correlation must be present in proton-neutron (p-n) pairs as well because of the isospin independence of the strong force. The present thesis is a study of the role the momentum correlation plays in deuteron production. Since the strong interaction is present regardless of thermal equilibrium and the strength of the momentum correlation is only a function of the source size, the deuteron yields provide a method of measuring the source size independent of the assumption of thermal equilibrium. Although there are large uncertainties associated with the proposed technique, some progress has been made beyond the purely statistical models reviewed in the previous section, by including the contributions from the strong interaction in deuteron production.

This study is done explicitly in the framework of Second Order Interferometry, which extracts the source size by fitting the measured correlation function with the theoretical prediction. A necessary requirement in obtaining the correlation function is the detection of two identical particles in the same event to plot their relative momentum distribution. Such a measurement is not possible using the deuterons alone, and one must instead consider the correlation functions for various source sizes and look at how the predictions for the deuteron yields change in order to extract the right source size. The use of the proton-

neutron correlation function to obtain the source size makes this analysis unique.

This thesis comprises five chapters and three appendices. Chapter 2 describes Experiment 866, including the hardware setup and the analysis procedures leading to the particle identification. Chapter 3 is the main body of the thesis where the theoretical aspects are discussed. It is here that the Second Order Interferometry is introduced and the concept of the correlation function is defined. Chapter 4 then discusses the results obtained based on the formalism developed in Chapter 3. The summary of the thesis is given in Chapter 5, which is followed by three appendices. The first presents the p, d, t, and ^{3}He spectra obtained from the ^{197}Au+^{197}Au collisions of three different centralities, while the other two present the calculation of the number of participants in the nuclear collision at a given impact parameter, and the derivation of the deuteron p_t spectrum from the proton p_t spectrum.

Chapter 2

Experiment

Experiment 866 (E866) at Brookhaven National Laboratory is an experiment designed to study semi-inclusive hadron production in nucleus-nucleus (A + A) collisions. E802 and E859, which preceded E866, have investigated a variety of collision systems ranging from p+^{9}Be all the way up to ^{28}Si+^{197}Au to understand the hadronic processes in a high baryon density environment. E866 is continuing the study with an even larger collision system, ^{197}Au+^{197}Au. In the most central Au+Au collisions, more than 350 nucleons participate in the collision, releasing an enormous amount of energy into the collision region and raising the nuclear matter density as much as ten times [Sch93]. Some workers believe that a new phase of matter (the quark-gluon plasma) would be created when matter is compressed to such a high density due to the asymptotic freedom of the strong force at small distances.

In order to obtain the Au beam, a dedicated ultra-high vacuum booster synchrotron had to be constructed between the Tandem Van de Graaff accelerator, where the Au ions are initially accelerated, and the AGS (Alternate Gradient Synchrotron) ring, which is responsible for accelerating the Au ions to the final momentum of 11.6 A·GeV/c. The booster is required in order to fully strip the electrons from the Au atoms before their injection into the AGS,* for the ions that are only partially stripped can collide with the residual gas molecules inside the ring,† and be deflected out of the ring by losing their electrons.

*More precisely, all electrons but two are stripped from the atom before the injection.

†The vacuum inside the ring is about 10^{-6} torr.

Once the Au beam has reached its final momentum in the AGS, it is extracted and bombarded on the ^{197}Au target with nominal thickness of 1.5%, 3%, or 4.5% interaction length in the E866 experimental area. Most of the data analyzed here were taken with the 1.5% target, which minimizes the multiple scattering of the produced particles inside the target. When the AGS is functioning at the optimum level, approximately a thousand beam bunches per hour, each containing about 3×10^4 Au projectiles, are extracted for collision. The beam intensity was restricted by the amount of radiation allowed in the experimental area. About 50 events are written to tape per spill for analysis. The data set analyzed here, obtained in 1992, comprises $\sim 5.5 \times 10^5$ SPEC events, which are the events with at least one charged particle within the spectrometer acceptance, containing $\sim 2.1 \times 10^5$ minimum bias protons and $\sim 1.9 \times 10^4$ minimum bias deuterons.

In central Au+Au collisions, roughly a thousand particles stream out from the collision region. An experiment to study collisions of such complexity requires a sophisticated tracking system to identify particles, detectors to describe event topology, as well as a reliable data acquisition system. In the following, a short account of the experimental apparatus is given and the analysis steps leading to particle identification are summarized.

2.1 Apparatus

2.1.1 Henry Higgins Spectrometer

The initial run of E866 was performed using the E859 detector configuration, which includes a 25 msr magnetic arm spectrometer,[‡] called the Henry Higgins (HH) spectrometer, supplemented with the 0° Fe-calorimeter (ZCAL) which serves as the global event characterizer, as shown in Fig. 2.1 [NIM90]. Mounted on the HH spectrometer are the HH magnet with an aperture of $84cm \times 42cm \times 240cm$ which can deliver field up to

[‡]For the run of October 1993, another spectrometer (FSPEC) with a smaller solid angle coverage, was built. FSPEC, located on the opposite side of the beam pipe from the HH spectrometer, is capable of operating in a higher multiplicity environment, and hence can swing to smaller angles with respect to the beam line to examine particle production in the more forward rapidity region in phase space.

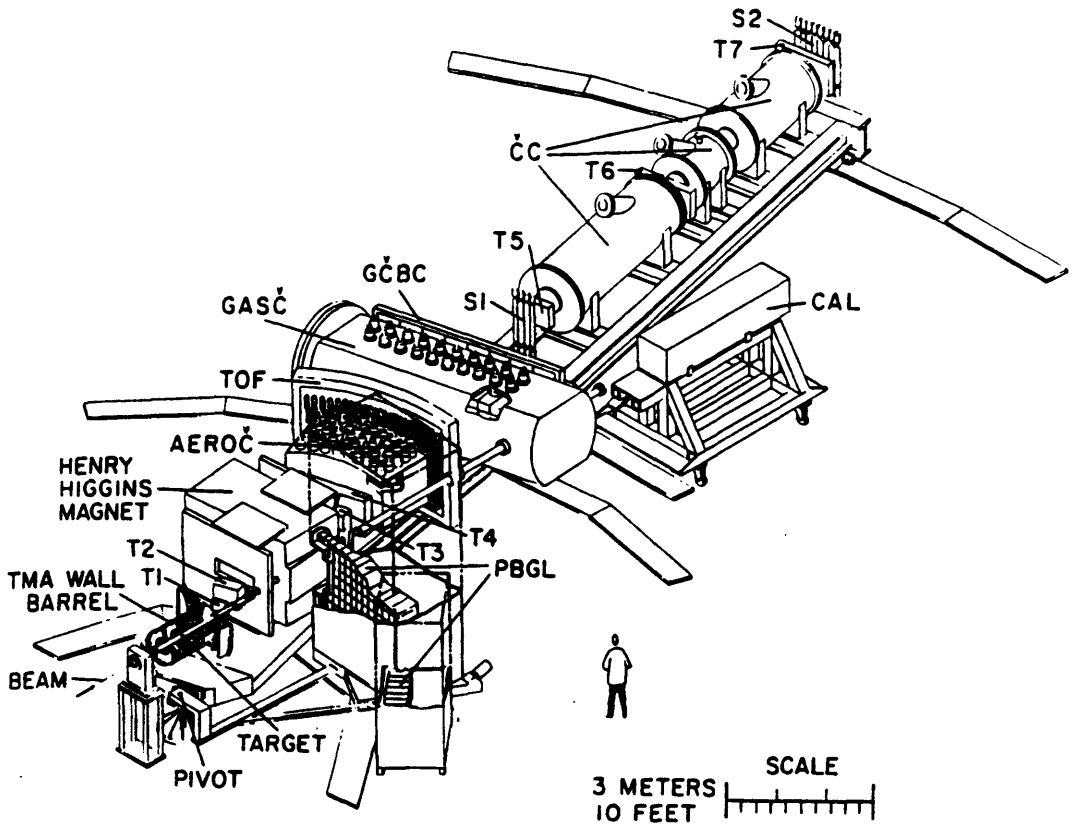

Figure 2.1: The E866(E802) Henry Higgins Spectrometer. The figure also shows a few detectors which were part of the E802/E859 setup but were removed for E866: PbGl array, TMA, and AEROČ.

$\int B_y dl$=1.46T·m [Col92, Vut92]; four sets of drift chambers for tracking, two (T1,T2) before and two (T3,T4) after the magnet; the time-of-flight wall (TOF), consisting of 160 slats of scintillator ($1.6cm \times 1.6cm \times 78cm$) read out by two PMT's, one at each end; and the segmented Gas Cerenkov (GASČ) counter behind the TOF wall, followed finally by the Back counter. The entire spectrometer arm can be rotated to different angle settings to study particle production in different rapidity regions.[§]

[§]Rapidity $y = \tanh^{-1}\beta$, $\beta = v/c$. See [Han90] for other commonly used relativistic kinematic variables.

2.1.2 Beam Counters

Upstream of the target, there is a set of plastic scintillators collectively called the Beam Counters. They define the beam, count the beam particles, and provide the start time for timing measurements in the experiment. At $10.6m$ downstream of the target is located another scintillator detector, called the Bull's-eye, which determines whether an interaction has taken place, by looking at the charge of the projectile spectator fragment. Because the energy deposited by the nucleus of charge Z in the scintillator is proportional to Z^2, which is sensitive to a change in Z, the Bull's-eye functions as the interaction trigger for the experiment. But the Au projectiles on a scintillator designed for the Si beam saturated the detector, so during the E866 running in 1992, the zero-degree calorimeter was used instead as the interaction trigger. As part of the upgrade to the experiment, the old Bull's-eye was replaced by a much thinner scintillator for the 1993 run.

2.1.3 ZCAL

ZCAL, which is located $11.7m$ downstream from the target, is an Fe-scintillator calorimeter, composed of 138 units of low-carbon steel absorber plates and scintillators stacked alternately to provide 8.9 interaction lengths for relativistic nucleons within 1.5° from the forward beam axis, [Bea89] i.e.

$$\tan^{-1}\frac{p_t}{p_z} \leq 1.5^\circ \quad , \quad p_t = \sqrt{p_x^2 + p_y^2}. \tag{2.1}$$

ZCAL measures the energy remaining in the projectile fragments proceeding at small angles downstream from the point of interaction. In a central collision, the overlap between the projectile and the target is extensive, and there is little energy left in the projectile fragment. The correlation between the energy measured by the calorimeter and the impact parameter of the collision makes such measurements important for event characterization.

One can enhance the statistics of the central events on tape by triggering on the events with the least ZCAL energies ($\overline{\text{ZCAL}}$). The events taken with the $\overline{\text{ZCAL}}$ trigger correspond

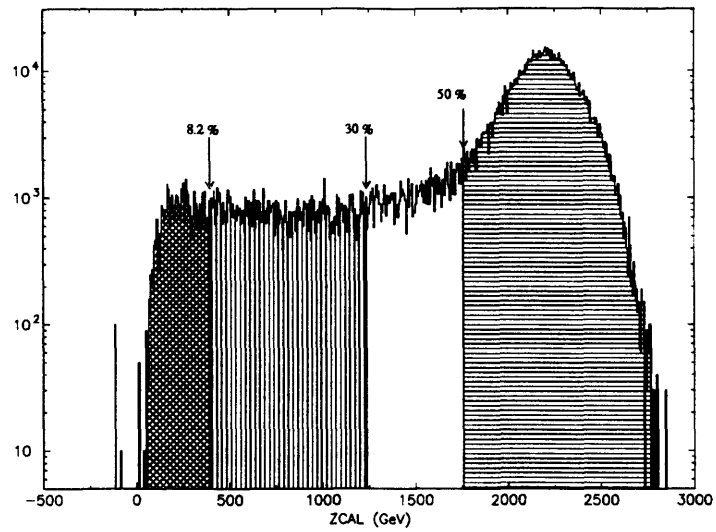

Figure 2.2: The ZCAL energy distribution for the interaction events. The arrows indicate the ZCAL cuts used for various centrality selection. The numbers refer to the corresponding percentage of the total cross section.

to the most central ~4% of the interaction cross section. However, the analysis for this thesis is based on the events collected with the SPEC trigger[¶] in order to minimize the possible systematic error when comparing the central and peripheral events, and the calorimeter output is used only to apply an off-line software cut on these events. Fig. 2.2 shows the distribution in the ZCAL energy for the interaction events and the software centrality cuts used in the analysis.

[¶]See p.16

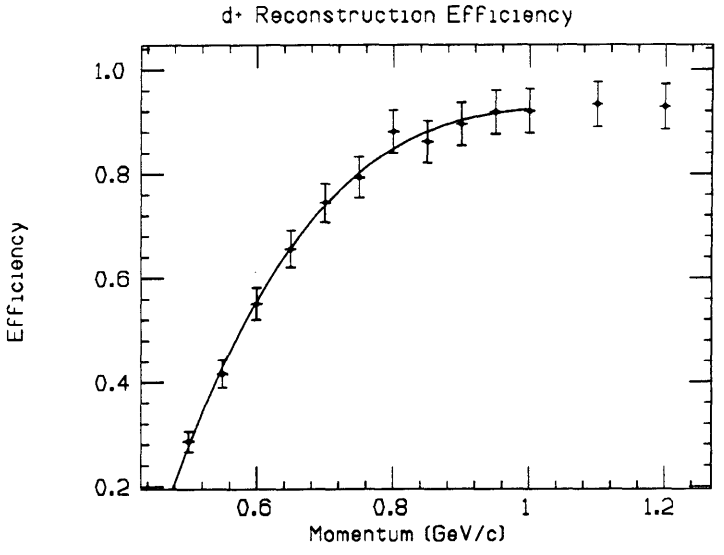

Figure 2.3: The deuteron reconstruction efficiency calculated by reconstructing the simulated deuterons of various momenta within the spectrometer acceptance. The points correspond to the calculated efficiencies. The line is a parameterized fit to these points. See text.

2.2 Passes

2.2.1 Track Reconstruction

The data reduction stage of the analysis consists of three passes: Pass0, Pass1/2, and Pass3. Each performs a well-defined set of tasks. Pass0 generates diagnostic histograms and obtains rough calibration constants for the different detector partitions; Pass1/2 translates electronic readouts to physical quantities and reconstructs particle tracks; and finally, Pass3 combines outputs from various detector partitions to make the PID decision. The purpose of these passes is to process the raw data on tape to more meaningful quantities so they can be easily manipulated in the Physics Analysis Workstation (PAW) environment. They are all performed within the CDF's Analysis Control Shell, which provides the framework for efficient memory management and data organization, while maintaining the modularity of individual detector partitions by permitting independent preparation of the analysis modules and assigning each of them a unique data bank.

Track reconstruction constitutes a major part of the analysis and takes the longest time to finish. For the data taken in 1992, there were two official track reconstruction algorithms—

Auscon and Trck3. All the particle spectra presented here are based on the tracks reconstructed by Auscon, but study shows both algorithms are comparable in efficiency [Ahl93]. The track reconstruction efficiency is a function of the particle momentum and the particle type. The major source of inefficiency is the multiple scattering the particles experience during their flight, particularly within the magnet. The amount of multiple scattering is proportional to $1/(p\beta)$, where p is the momentum and $\beta = v/c$, and is by far the biggest problem for low momentum particles of large mass. In the presence of large multiple scattering, the algorithm is unable to associate the particle track behind the magnet with the right hits in front of the magnet, thus resulting in track loss. One must correct for such inefficiency through a simulation study. Fig. 2.3 is an example of the deuteron reconstruction efficiency estimated by generating simulated deuterons of various momenta within the spectrometer acceptance and by calculating their reconstruction rate. Each point corresponds to a separate simulation study. The line (in this case a fourth order polynomial) is a parameterized fit through these points which is used by the cross-section generation code to correct for the reconstruction inefficiency. At momenta greater than 1 GeV/c, the efficiency is assumed to be a constant and equal to the value at 1 GeV/c.

Similar studies must be done for other particle types because the reconstruction efficiency depends on the particle type. For instance, the protons have a higher reconstruction efficiency than the deuterons of the same momentum, which in turn are more efficiently reconstructed than the tritons, and so on. Also, the reconstruction efficiency is a monotonically decreasing function of the multiplicity of charged particles within the spectrometer. The decrease in efficiency with the multiplicity is about 1.2% for each additional particle within the spectrometer in a given event. The study was done only up to multiplicity 5, but during the particle cross-section generation, the correction is extrapolated to higher multiplicities.

2.2.2 Particle Identification

Particle Identification (PID) in E866 relies primarily on momentum measurement followed by time-of-flight measurement provided by the TOF wall, located $6.5m$ from the target. During the track reconstruction stage of data analysis, the path lengths of individual particles from the target to the TOF wall are determined. The path length varies with the particle momentum because the amount of bending inside the magnet is a function of momentum. Time-of-flight measurement gives the particle velocity, and the momentum and the velocity together then fix the particle mass.

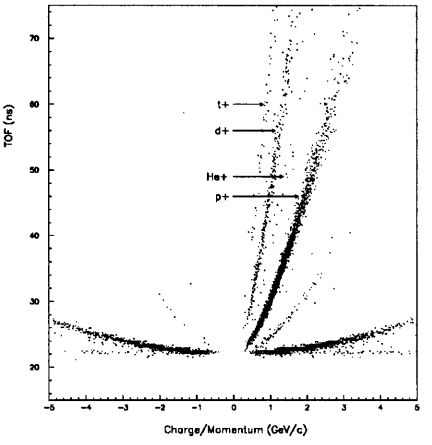

Figure 2.4: Particle identification from TOF and p measurements. From Run 11277.

However, the TOF wall has a finite timing resolution of $\sigma_{tof} \simeq 120$ ps, and one gets a distribution in time of flight, rather than a single number, for a given momentum. Cuts are made in p–$1/\beta$ space with 3σ uncertainty in $1/\beta$ for a given $p \pm \delta p$. For high momentum particles the TOF wall information is inadequate to separate different particle species. The protons with momentum above 3.4 GeV/c, for instance, cannot be differentiated from the pions. When this happens, the GASČ makes the PID decision based on the Čerenkov emission by the pions. Other ambiguities cannot be resolved by the GASČ for the particle's velocity is not high enough. For the clusters, the following hold true: When the regions in

p-$1/\beta$ space for the deuterons and the protons start overlapping, the deuterons stop being identified; when the deuteron and the triton regions overlap, the tritons stop being identified; and when the deuteron and ^{3}He overlap, the ^{3}He stop being identified. This is to minimize the systematic error from misidentifying more abundant particles as the rarer particles. The energy loss in the TOF slats, which is measured by the photomultipliers mounted on the two ends of each slat, is used to make a charge cut in the regions where the protons and deuterons overlap with the ^{3}He. As a result of the charge cut, a small percentage (on the order of one percent) of the candidates for the protons and deuterons are discarded. See Fig. 2.5 for a summary of the cuts used for particle identification in E866.

Since the curvature of the particle track inside the magnetic field is proportional to the momentum divided by the charge, two particles with the same p-to-charge ratio cannot be distinguished from each other by their tracks alone. In some cases, the time-of-flight can be used to identify the particle, but the velocity of the deuteron with a given momentum is the same as that of an α with twice the momentum, hence neither the curvature of the track nor the TOF is of any use in telling the two apart. The only way to separate the deuterons from the α's is by the energy loss the particle experiences inside the TOF slats. By the well-known Bethe-Bloch formula [Leo87], the α would lose four times the energy the deuteron loses over the same distance. [Sar89] reported the α abundance to be around 1% of the deuterons in Si+Au collisions; it is higher for backward rapidities and smaller for the more central rapidities. The energy loss spectra of the entire set of p, d, t, and ^{3}He used in the analysis are shown in Fig. 2.6. There is what seems to be a "bump" in the deuteron spectrum around 1000,[‖] which is not found in the other three plots. This bump may correspond to the α's. The upper limit on the contamination from the α's in the particles identified as deuterons is estimated to be around 2.2% by counting the deuterons which are assigned a charge greater than one based on the TOF slat read-out. But it is doubtful that all these deuterons are α's, for the energy loss distribution has a long tail which can make a particle of charge one look

[‖]See the caption for Fig. 2.6 for an explanation of the scale used in the plot.

as if it had a charge two. A similar counting reveals that around 1.3% of the protons are assigned a charge equal to two or higher. Hence, a more accurate estimate of the number of α's among the deuterons would be the difference of the two, i.e. around 1%. Since there are other larger systematic uncertainties in the analysis, no further effort was made to identify the α's among the deuterons. As a reference, there are 733 ^{3}He, 1906 t, 19,098 deuterons, and 214,016 protons in the entire data set.

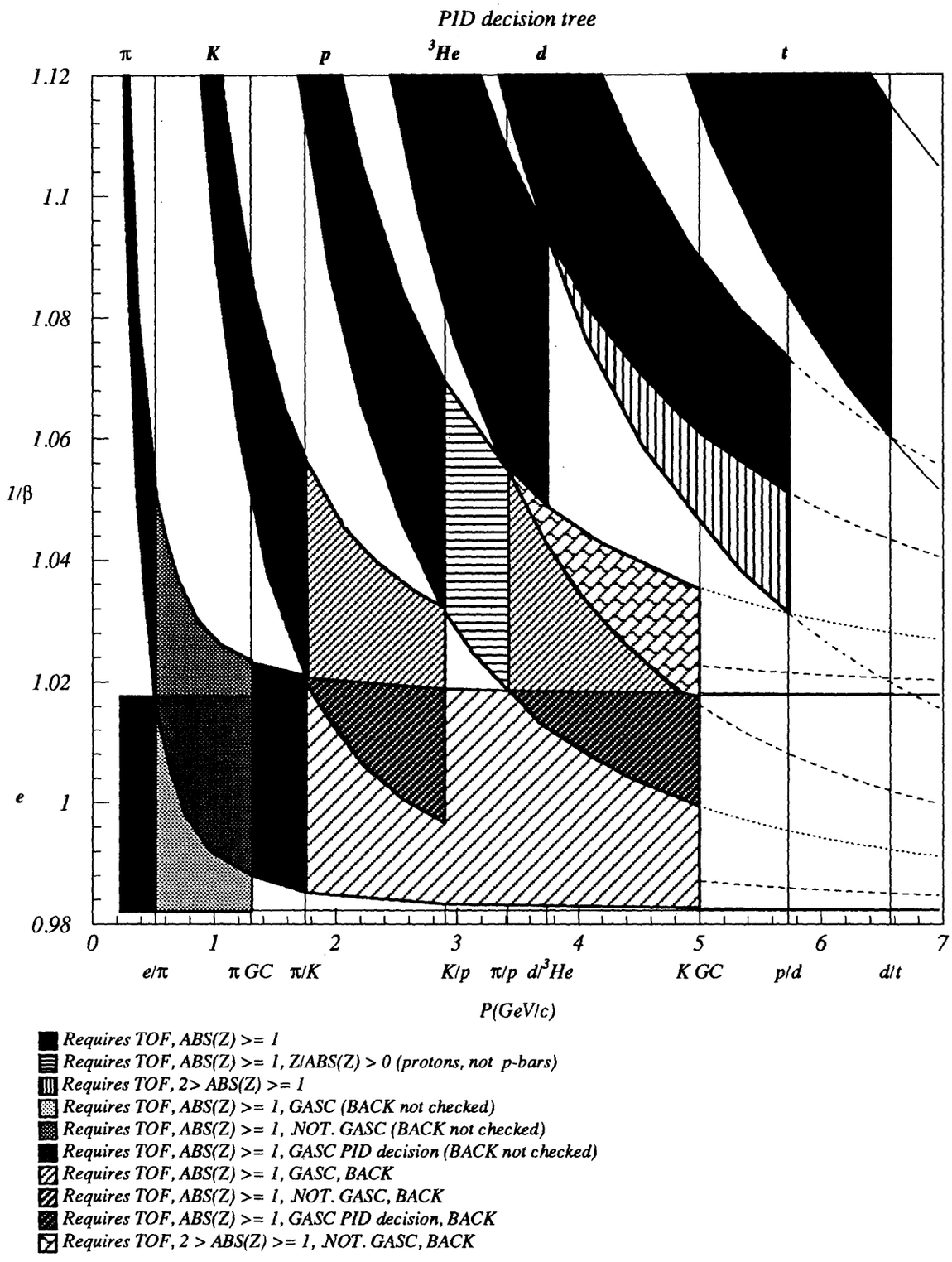

Figure 2.5: A graphical representation of the PID algorithm used during Pass3 to make the PID decision.

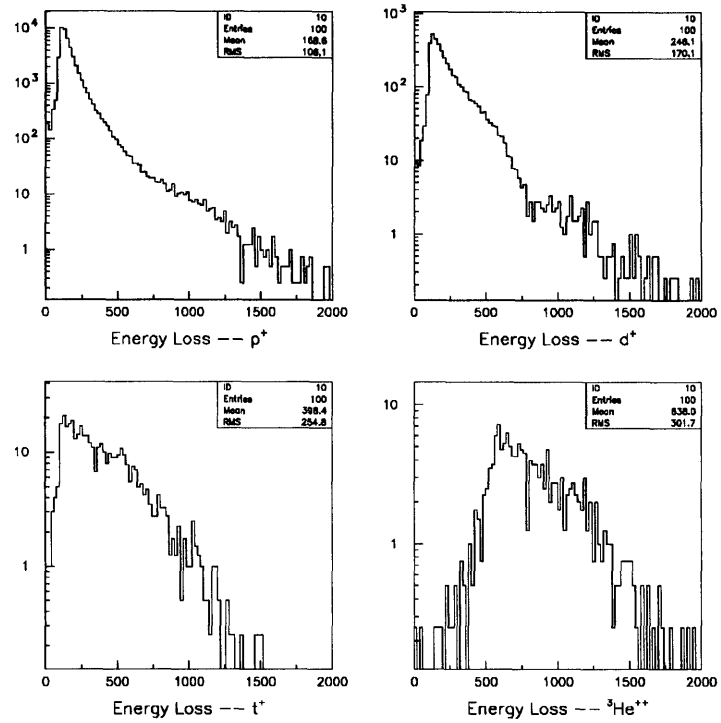

Figure 2.6: The distributions of the energy loss suffered by the particles inside the TOF slats. The abscissa is in an arbitrary scale so that the distribution of the minimum ionizing particles has the peak at 100.

Chapter 3

Analysis

3.1 Overview

The one-pion exchange potential, which dominates the nuclear interaction at distances greater than 2 fm, is an attractive potential [Won90]. As a result, the relative momentum between a pair of nucleons emitted from a common source, averaged over all pairs, is smaller than it is in the absence of such an attractive potential. This has a favorable consequence for deuteron (and heavier cluster) formation, since the constituent nucleons must have a small relative momentum in order to form a bound state. If the attraction is large then there would be many more proton-neutron pairs with a small relative momentum, and the overall probability of some of them forming deuterons would also be greater. When the average nucleon separation inside the source is smaller than 2 fm, the nuclear interaction is dominated by two-pion and heavier meson exchanges. The attraction is stronger for these intermediate regions of separation and hence an even larger increase in the population of low-q* pairs is expected. On the other hand, at much smaller separation ($\leq$ 1 fm) there is hard-core repulsion arising from multi-pion exchange as well as QCD effects. Therefore, the source size is an important parameter in determining the extent of modification of the q-distribution and therefore in determining the deuteron production rate.

One way to quantify the extent of enhancement observed at low-q is to derive the corre-

*The variable $q = |\Delta\vec{p}/2|$ is used in the study for historical reasons. Physically, it corresponds to the magnitude of the momentum of each nucleon in the CM system of the pair.

lation function (CF). The correlation function is the ratio ACT/BCK, of the q-distribution one ACTually observes in an experiment to the BaCKground q-distribution one would have observed if the distribution were strictly statistical, i.e. the q-distribution determined purely by the single particle distribution without any dynamical effect that might favor one value of q over another. A rise above one in the CF indicates enhancement, while suppression is manifested by a fall in the CF. Since the total number of pairs in a given event is conserved, an enhancement at low q implies the suppression at high q. While this is mathematically true, the low-q enhancement is usually limited to about $q \leq 50$ MeV/c, which includes only a tiny fraction of the entire set of the nucleon pairs; hence the change in the overall normalization is insignificant. In other words, one can always assume the correlation function approaches 1 for large q.

3.2 Interferometry

The correlation function first appeared in the context of Second Order Interferometry, involving two identical unbound particles. Since the deuteron analysis in this thesis derives its theoretical formalism from Interferometry, an introduction to the topic is a worthwhile digression. However, only a sketchy introduction is given, for the purpose of this section is to create a suitable context for the presentation of new results rather than to have a complete discussion of Interferometry. If desired, details can be found in the references cited below.

There are two types of Interferometry— also referred to as Identical Particle Correlation in the literature. One of them deals with two identical bosons, the other with two identical fermions. The name refers to the fact that the probability of observing a pair of identical particles with the relative momentum q is modified due to the interference between the two particles. This is different from the better known interference effects in quantum mechanics, such as the electron diffraction in which the probability of a certain outcome is influenced by the electron interfering with itself. In Interferometry, a completely coherent source does not manifest an interference effect, while in the latter case, the interference exists only among

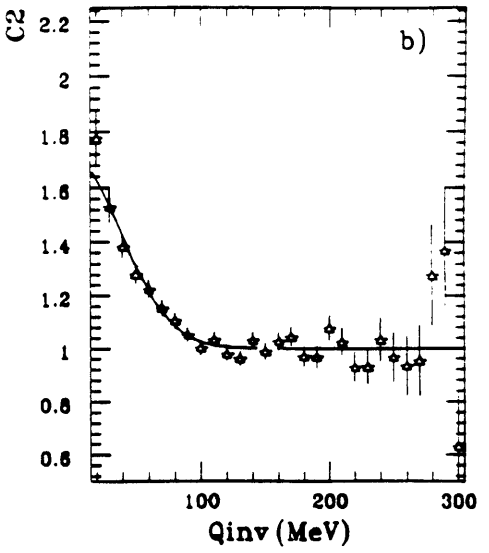

Figure 3.1: The correlation function for ^{28}Si+^{27}Al $\longrightarrow 2\pi^- + X$. (From [Mor90].)

coherent sources.

Bose-Einstein (BE) Correlation

[Kop77, Pra84, Bar86, Zaj88, Mor90, and references therein.]

The Bose-Einstein correlation refers to the low-q enhancement observed for pairs of identical bosons from the same event, over the pairs obtained by mixing the particles from different events. In the latter case, the particles cannot interact with one another for they come from different events, and their q-distribution is purely statistical. When two identical bosons, say π^+'s, are emitted from two spatial points $\vec{r}_1$ and $\vec{r}_2$ within the source with momenta p_1 and p_2, an observer cannot determine which one came from $\vec{r}_1$ and which from $\vec{r}_2$ just by observing their momenta. So the total wave function must contain both amplitudes corresponding to the two possible permutations of the spatial coordinates between the particles. This is the well-known requirement that the total wave function of a pair of identical bosons must be symmetric under exchange of the particles. Since the probability is given by the square of the wave function, the probability distribution then contains an interference term, which modifies its distribution. The interference term turns out to be the square of the Fourier

transform of the source distribution with respect to the relative momentum of the particles,

$$C \equiv \frac{ACT}{BCK} = \frac{P(p_1, p_2)}{P(p_1)P(p_2)} = 1 + \mid \tilde{\rho}(q) \mid^2, \tag{3.1}$$

where $\tilde{\rho}(q)$ is the Fourier transform of the source distribution. $|\tilde{\rho}(q)|^2$ becomes zero for large q, regardless of the source shape. Compared to the probability distribution corresponding to an unsymmetrized wave function (BCK), therefore, the distribution for the symmetrized wave function(ACT) has an enhancement at low q.

Theoretically, the momentum correlation can arise from the strong interaction, the Coulomb interaction, and the symmetrization of the wave function. In both π-π and K-K correlation studies, the contribution from the strong interaction is estimated to be small [RV93]. The Coulomb interaction, which is repulsive for a pair of identical, charged particles, suppresses the correlation at low relative momentum and creates a hole at $q \simeq 0$. The Coulomb contribution to the correlation function consists of three parts: 1. The Gamow factor, which is defined as the ratio of relative wave functions with and without the Coulomb interaction in the limit of a point charge source. 2. The finite source size correction which is on the order of the source size divided by the Bohr radius of the particles. 3. The screening effect due to "spectator" charges found between two points of emission $\vec{r}_1$ and $\vec{r}_2$ [Rol93].

A typical Bose-Einstein correlation function is shown in Fig. 3.1, where a gaussian source distribution in the coordinate space is assumed. The gaussian is commonly used for the source distribution because its Fourier transform, conveniently, is also the gaussian, making algebra simple. The choice of a gaussian also reflects our ignorance of its shape. It is normalized to one in the absence of a correlation. The source size is extracted by fitting the CF to the data.

$$C_2^{fit} = N(1 + \alpha Q_{inv})(1 + \lambda exp(-Q_{inv}^2 R^2/2)), \tag{3.2}$$

where

$$Q_{inv}^2 = \mid \Delta\vec{p} \mid^2 - \mid \Delta p_0 \mid^2 \longrightarrow q^2 \text{ in the CM.}$$

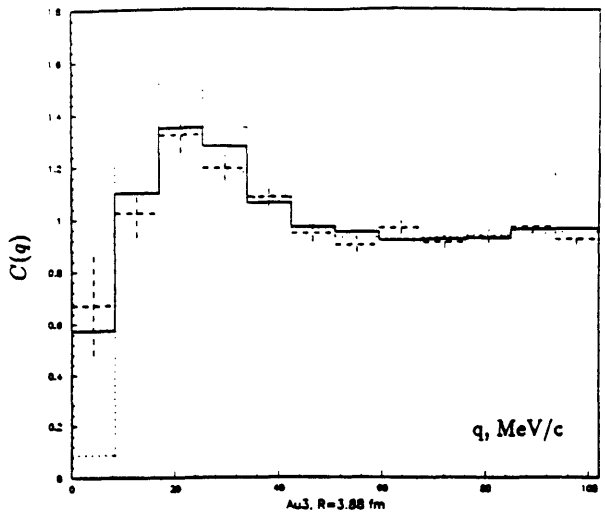

Figure 3.2: The correlation function for ^{28}Si+^{197}Au $\longrightarrow 2p + X$. (From [Vut92].)

The source is then described by

$$\rho(x) = exp(-x_\mu x^\mu / R^2). \tag{3.3}$$

Proton-Proton Correlation

[Pra87, Dup88, Gon91, Vut92, Kun93, and references therein.]

The correlation study of two identical fermions is exemplified by two-proton interferometry. Contrary to the case of two pions, here the total wave function has to be antisymmetric under exchange of the particles. Other differences include the dominant contribution from the strong interaction, the Coulomb hole which extends farther out in q than for π-π pairs, and a larger correction due to finite size of the source. Combined, they produce a CF which looks quite different from a π-π correlation function. A proton-proton CF obtained from the study of ^{28}Si+^{197}Au is shown in Fig. 3.2. Again the assumed source distribution is a gaussian. The fitting parameters for the two-proton correlation measument are the overall normalization and the RMS (radius) of the source assuming zero lifetime.[†]

[†]The reason for assuming zero lifetime is the correlation function cannot discriminate an elongated source from a long-lived spherical source. See §2.3.1 and §7.2 in [Vut92] for more discussion on zero lifetime.

3.3 Proton-Neutron Correlation

E866 and other relativistic heavy ion experiments at present do not directly measure the neutrons to allow the study of the proton-neutron correlation at low q. Apart from the experimental difficulties of obtaining the actual proton-neutron q-distribution, the study of the proton-neutron correlation also differs from both the π-π and the p-p correlations in that the proton and the neutron may form a stable bound state, while no bound state is known for the pion or the proton pairs. Therefore, even if one were to measure the proton-neutron q-distribution it is not clear whether the formalism of the Second Order Interferometry can be directly applied to the proton-neutron correlation to extract the source size.

Despite this difference between the p-p correlation and the p-n correlation, the idea of the correlation function is still very useful because of the intrinsic one-to-one relationship between the correlation function and the actual q-distribution. The proportionality is given by the background distribution, which can be generated from any two particles as long as they have the same production mechanism as the protons and the neutrons, and their momenta are uncorrelated. Because of the direct relationship between the correlation function and the actual distribution, one can effectively carry out the Interferometry measurement in reverse, by starting with the correlation functions, multiplying it by the background to get the "actual" distributions, which are compared with some observable from the experiment.

Since E866 does not measure the actual proton-neutron q-distribution, one must answer first what observable can be compared with the "actual" distribution one presumably derives from the background and the proton-neutron correlation function. The most obvious choice is the integrated deuteron yields dN/dy, though the p_t distribution is also a possibility. In either case the extraction of the source size involves several independent preparatory steps. First, the proton-neutron correlation function must be derived for several source sizes and the background must be generated in such a way that it contains the right number of proton-neutron pairs but no momentum correlation within the pairs. Then we must coalesce the proton-neutron pairs in phase space in order to compare with the measured deuteron

dN/dy, which requires introducing the upper momentum cut and the upper spatial cut. These procedures are described one at a time in the following sections.

3.4 Proton-Neutron Correlation Function

The p-n correlation function is available through Scott Pratt's code, [Pra92] which is also responsible for generating the p-p correlation function used in [Vut92]. This code calculates the CF for a gaussian source with a given RMS. The correlation function thus calculated is independent of the single particle spectrum and the only parameter that enters its derivation is the source size. Though one hopes to relate the source size to the correlation function in a straightforward manner, this approach may be flawed because of the possible existence of the dynamical correlation between the momentum and spatial variables, which some phenomenological models of the nuclear collision predict. One can also take the simulated particle events containing the momentum and spatial informations of the particles, and calculate the correlation function based on them. This method has the advantage that the dynamical correlation is explicitly conserved when the correlation function is calculated, so that one can be sure that the correlation function thus obtained always has the right amount of dynamical correlation predicted by that particular event generator.

However, by obtaining the correlation function by the second method, one loses the control over the source size. When both the momentum and spatial variables are supplied by the collision model for the calculation of the correlation function, the user cannot associate the correlation function with the source of a given size and shape. It is only by separating the spatial and momentum variables that one has the knowledge about the source size. Though this separation necessarily takes the dynamical correlation out during the CF calculation, it is more relavant to the present study, where it is critical to know which correlation function corresponds to which source to be able to extract the size from the deuteron dN/dy. Since the dynamical correlation has not been included in the derivation of the correlation function, it must be put in by hand. This will be a source of uncertainty in the analysis, but hopefully

it can be minimized in the future, when our understanding of the dynamical correlation has sufficiently advanced.

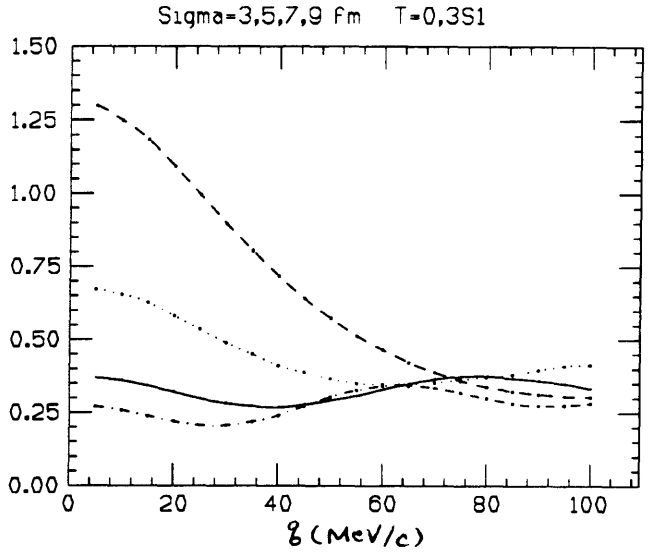

Figure 3.3: The contribution to the p-n correlation function from $^3S_1$ channel for σ_{source}=3 fm(dash), 5 fm(dotted), 7 fm(solid) 9 fm(dot-dash).

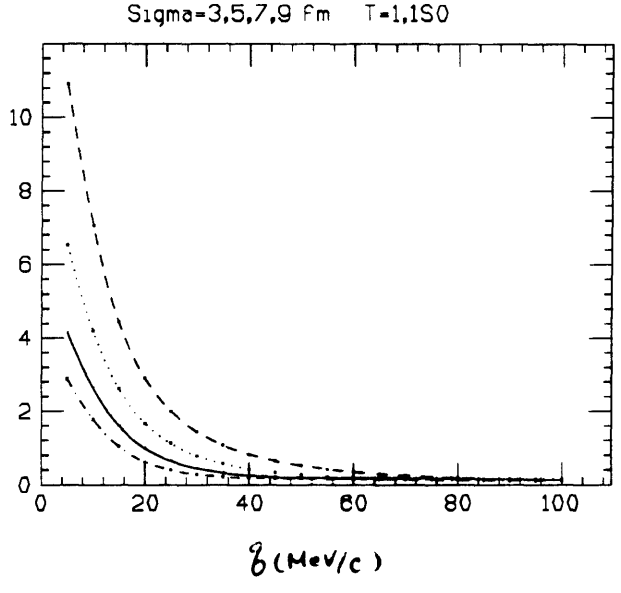

Figure 3.4: The contribution to the p-n correlation function from $^1S_0$ channel for for σ_{source}=3 fm(dash), 5 fm(dotted), 7 fm(solid) 9 fm(dot-dash).

The computation leading to the CF is based on a partial wave analysis of nucleon scattering in the pair's CM system. By the well known formalism, for a central potential, one can

decompose the scattering amplitude into contributions from different angular momentum channels,

$$f(\theta) = \frac{\sqrt{4\pi}}{k} \sum_{\ell=0}^{\infty} \sqrt{2\ell+1} e^{i\delta_\ell} \sin\delta_\ell Y_{\ell 0}(\theta), \tag{3.4}$$

where δ_ℓ is the phase shift for the ℓ-th channel. Imagine a p-n pair whose relative wave function is $\psi(r_0, q)$, where $r_0 = (|\vec{r_0}|)$ is their spatial separation at $t = 0$ and q is the magnitude of the momentum difference divided by 2. The proton-neutron scattering can be treated as a one-body problem with a reduced mass in an effective potential, which is parameterized to reproduce the observed phase shifts. Then, phase shifts due to scattering against this parameterized potential are calculated for S- and P- channels by comparing $\psi(r_0, q)$ with its asymptotic form $\psi(r, q)$ as $r \to \infty$. The derivative of the phase shifts with respect to q is sufficient to calculate the enhancement in the correlation function, i.e. $\Delta C(q) = C(q) - 1$ [Boa90,Vut92]. Hence, independent of the single particle momentum distribution, the CF can be calculated just by knowing the spatial distribution of the particles, or equivalently by specifying the RMS of a gaussian distribution. The rationale for using only two channels $\ell = 0, 1$ is that for momentum q, only channels up to $\ell \leq rq$ experience any significant phase shift, and here we are interested in low-q scattering that is most pertinent to deuteron production.

Being fermions, a proton and a neutron have a half-integer spin, $s{=}\frac{1}{2}$. In addition, each possesses an isospin $t{=}\frac{1}{2}$. In fact, the proton and the neutron are the two isospin projection states of a $t{=}\frac{1}{2}$ particle, the nucleon: the proton being the $t_z{=}{+}\frac{1}{2}$ state and the neutron being the $t_z{=}{-}\frac{1}{2}$ state. A p-n scattering, then, can go through four different channels: (T,S)=(0,0), (0,1), (1,0), (1,1), where T= $t_1 + t_2$ and S= $s_1 + s_2$ are the total isospin and spin for the pair, respectively. By conservation of isospin in the strong interaction, there is no operator connecting the initial and final states of different isospin. Furthermore, once isospin is included to label the pair's quantum state, the total wave function of the pair must be antisymmetrized under exchange of the particles. This is, however, different from saying that a proton-neutron pair must have an antisymmetrized wave function! Antisymmetrization is

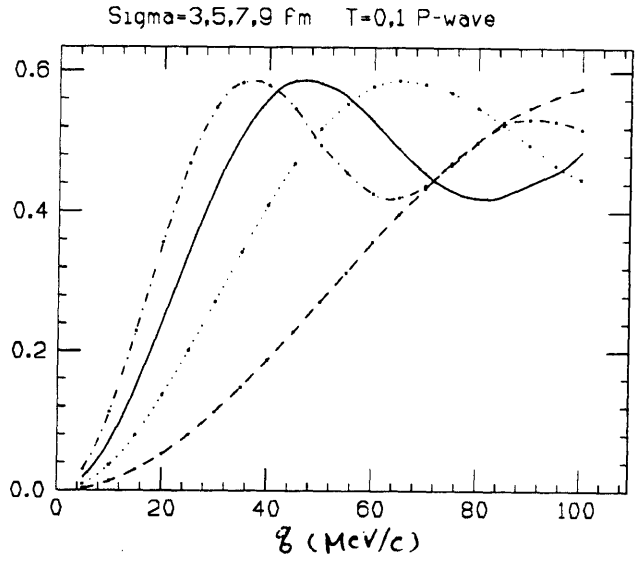

Figure 3.5: The contribution to p-n CF from two antisymmetric channels for σ_{source}=3 fm(dash), 5 fm(dotted), 7 fm(solid) 9 fm(dot-dash).

required if the total isospin is specified, but an unbound p-n pair is always a mixed state of T=0 and T=1. For a fixed T, the antisymmetrization requirement assigns different orbital angular momenta ℓ to spin states 0 and 1, and hence the two spin states with the same isospin are decoupled due to parity conservation. We thus arrive at the overall simplifying conclusion that these four channels are all independent of one another and the total CF is just the sum of the individual contributions. Table 3.1 lists these channels, with their relative weights. Contrary to naive expectation, the channels (T,S)=(1,0) and (1,1) have weights of

T	S	L	Rel. wgt.	$^{2S+1}L_J$
0	0	1	1	$^1P_1$
	1	0	3	$^3S_1$
1	0	0	1	$^1S_0$
	1	1	3	$^3P_{0,1,2}$

Table 3.1: Channels available in p-n scattering

1 and 3, rather than 3 and 9, obtained by multiplying an isospin triplet with a spin singlet and a spin triplet. This is because a p-n pair may be part of an isospin triplet but the third component of the total isospin T_z is 0, regardless of whether T=0 or 1. Hence, both T=0

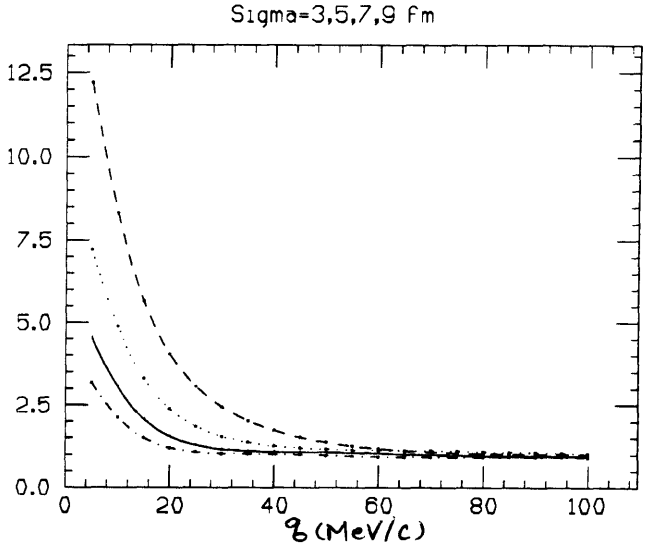

Figure 3.6: The total p-n CF for σ_{source}=3 fm(dash), 5 fm(dotted), 7 fm(solid) 9 fm(dot-dash).

and T=1 carry equal relative weight. Overall weights for channels with a symmetric ($\ell = 0$) and an antisymmetric ($\ell = 1$) spatial part are 4:4, making the p-n pair wave function neither symmetric nor antisymmetric under particle exchange. Figs. 3.3 - 3.6 explicitly show the contribution to the total correlation function from each channel.

3.5 Background Generation

It is important to generate a reliable background because of the critical role it plays in connecting the correlation function to the "actual" q-distribution. In principle there are two ways to generate the background. One of them is to use the protons measured in the experiment. Because the spectrometer acceptance is less than 4π, one has to deconvolute the measured proton distribution in order to get the true distribution; this is routinely done during single particle inclusive cross-section measurements. Next, we assume that the neutron distribution can be obtained by scaling from the proton distribution. Finally, the momentum difference of each proton and each neutron computed in their CM system gives the background q-distribution. The background is not entirely devoid of correlation, for the measured single particle proton spectrum has already been distorted by p-p correlations (see

[Mor90] for more on residual correlations in the background), but more importantly this method may have difficulty in getting the right number of total p-n pairs in the background, because the total number of neutrons is not well known. The only constraint on its number is that the sum of all protons, neutrons, and other baryons must add up the number we started with, i.e. $394 = 2 \times 197$. Because the initial abundance of the neutrons is greater than that of the protons, the charged pions created in the collisions are more likely to collide with the neutrons and convert them to protons than to convert protons to neutrons. Thus, the net effect is a shift toward equilibration in particle numbers. Just how far the equilibration proceeds is not clear. Though the proton abundance can be experimentally determined, its dN/dy then becomes unduly important for the analysis. Furthermore, we also require the dN/dy's of the Λ's and Σ's as well, to be able to deduce the abundance of the neutrons accurately. All in all, this method introduces unnecessary complication to the study of deuteron production.

An alternative method, which was used in the present work, is to invoke a model that successfully reproduces the single particle proton distribution. By isospin symmetry of the strong force, we can say without being too speculative that it would also fit the neutron distribution well, if it were experimentally measured. Again a p-n pair is Lorentz boosted to its CM system before q is computed. The Lorentz transform is achieved by: [Jac75]

$$\begin{aligned} \vec{p}_{CM} &= \vec{p} + \frac{\gamma_{CM} - 1}{\beta_{CM}^2}(\vec{\beta} \cdot \vec{p})\vec{\beta} - \gamma\vec{\beta}p_0, \\ \vec{\beta} &= \frac{\vec{P}}{P_0}, \\ (P_0, \vec{P}) &= p_{prot} + p_{neut} \quad \text{(both four vectors.)} \end{aligned} \tag{3.5}$$

A hadronic cascade code developed at Brookhaven, ARC (A Relativistic Cascade), was chosen to generate the p-n background because of its [reasonable] success in simulating the proton rapidity distribution dN/dy in ^{197}Au+^{197}Au collisions at 11.6 A·GeV/c. See Fig. 3.7(a). Agreement with E802 proton data from ^{28}Si+^{197}Au at 14.6 A·GeV/c has also been tested independently [Pan92]. That this code was specifically designed to work at the AGS en-

ergy and simulated data from ARC were available early on were also important reasons for choosing this code over others. Nevertheless, as Fig. 3.7(b) shows, there is still some discrepancy between data and the theoretical prediction in the shape of the p_t distribution. The smaller inverse slope predicted by the ARC raises the number of p-n pairs with small q in the background, and consequently the final deuteron dN/dy as well.

The proton temperatures predicted by ARC for the collisions with impact-parameter less than 4 fm are given in Table 3.2 for the rapidity bins of width 0.1 from [0.2,0.3] to [1.4,1.5]. They are much smaller than the values measured by E866 for the central-most 8.2% of the inelastic collisions. See Fig. A.4 in Appendix A.

Rapidity	$T \pm \Delta T$ (GeV)
[0.2,0.3]	0.113 ± 0.013
[0.4,0.5]	0.152 ± 0.014
[0.6,0.7]	0.176 ± 0.016
[0.8,0.9]	0.192 ± 0.017
[1.0,1.1]	0.202 ± 0.017
[1.2,1.3]	0.212 ± 0.017
[1.4,1.5]	0.218 ± 0.017

Table 3.2: The proton temperatures predicted by ARC.

3.7 Momentum Cut

Once the proton-neutron CF and the background have been generated, the "actual" distribution is readily obtained by multiplying the two. Fig. 3.8 is an example of the "actual" distribution for the rapidity window y=[1.0,1.25] obtained by distorting the background with the correlation function corresponding to various source parameters σ_{source}, which is related to the source size by a multiplicative factor. The enhancement is larger for a smaller σ_{source}, as one expects intuitively, if the interaction is due to an attractive potential. It is important to note that this source parameter is different from the actual source radius, when comparing it to values from other measurements. σ_{source} used in [Pra92] is the RMS rasius of the

magnitude of the spatial separation between two randomly selected emission points. The RMS radius of the gaussian describing the distribution of the emission points themselves is given by RMS $= \sqrt{3/2} \times \sigma_{source}$.

In order to compare the ACT with the deuteron distribution, one must decide on a *momentum cut.* By this is meant that there is a maximum q allowed, q_{cut}, above which a p-n pair is forbidden to form a deuteron. This is a simplified picture of what must really happen during coalescence, because it is conceivable that occasionally a p-n pair with $q \geq q_{cut}$ manages to form a bound state though the odds are against it. A more sophisticated model would convolute the momentum part of the deuteron wave function to the q-distribution in order to account for such possibilities. A more difficult question in applying a hard momentum cut is to decide on the value of q_{cut}. In order to find a reasonable value for q_{cut}, we approximate the potential inside the deuteron with a square well of the form, $V(r) = -V_0\theta(a-r)$, where r is the relative distance and a is the maximum separation between the proton and the neutron, which is set to 3 fm. (See Fig. 3.9.) The ground state energy is calculated by solving the Schroedinger equation with appropriate boundary conditions. Explicitly, the equations to be solved are

$$A \sin ka = B \exp(-\kappa a) \tag{3.6}$$

$$-Ak \cos ka = -B\kappa \exp(-\kappa a), \tag{3.7}$$

where

$$\frac{\hbar^2 k^2}{2\mu} = V_0 - E_{BE}$$

$$\frac{\hbar^2 \kappa^2}{2\mu} = E_{BE}$$

$$E_{BE} = \text{deuteron binding energy} = 2.2 \text{ MeV}$$

$$V_0 = \text{the depth of the square potential well.}$$

Dividing Eq. 3.6 by Eq. 3.7 and numerically solving the resulting transcendental equation gives $\hbar k$=60MeV/c; q_{cut} is set to this k. Its physical meaning is that a nucleon which

will ultimately form a deuteron cannot have the kinetic energy in the CM system greater than the kinetic energy in the ground state of the deuteron. Whether it is justified to set q_{cut} to this value is arguable, and indeed other workers have used different q_{cut}'s [Bal93]. Important to note, however, is that: 1. This value of q_{cut} is not unreasonable for the simplified calculation we are doing here, and as mentioned before, the correct implementation probably requires using the deuteron wave function. Most likely the q_{cut} depends on the spatial separation, because the inter-nucleon potential is a function of spatial coordinates. 2. Unlike the Coalescence Model, where the momentum cut p_0 is a parameter (see p. 10) to be fitted by the deuteron dN/dy, our q_{cut} is fixed from the outset by a physical argument.

3.7 Spatial Cut and Dynamical Correlation

Those p-n pairs which have passed the momentum cut are then subjected to a spatial cut. As with the momentum cut, this is based on a physical argument that the proton and the neutron must originate from spatial points that are *not too far* from each other in order to form a deuteron. The "closeness" is defined as a hard spatial cut with the upper bound of 3 fm, i.e. a p-n pair is given the weight $w = \theta(r_{cut} - \Delta r)$, $\Delta r = |\Delta\vec{r}|$. $r_{cut} = 3$ fm. Once a p-n pair has passed the momentum and the spatial cuts, it is regarded as a deuteron and the collection of such pairs are compared with the measured deuteron dN/dy.

Because the spatial separation of the pairs $\Delta\vec{r}$ is randomly sampled from the gaussian, it is independent of the relative momentum q and is represented by a single number for a given source size. The number is obtained by calculating the probability that a randomly selected proton-neutron pair has the spatial separation less than r_{cut}, when the they are distributed according the gaussian of a given RMS centered at the origin. One might try to restore some of the correlation between the variables by putting it in by hand. But the dynamical correlation is a difficult quantity to estimate and to implement. The only way to do it consistently is to rely on the event generator to tell us explicitly how they are related.

To see where dynamical correlation comes from, we need only think about particle emis-

sion following a nuclear collision. Particles, irrespective of particle type, are preferentially emitted normal to the surface of the source. Though one must make allowance for emission at angles other than 90°, it is likely that a pair that has a small q also has a small $\Delta\vec{r}$, because they are more or less emitted at a normal angle. Even though it could so happen that two nucleons which are emitted from points in space located diametrically opposite to each other within the source can have a very small q if they are both emitted almost tangentially to the surface, this is unlikely due to the dynamical correlation.

A general physics consideration, therefore, shows that a proton-neutron pair that has passed the q_{cut} should come from the spatial points $\vec{r}_1$ and $\vec{r}_2$ which are closer to each other than if they had a large relative momentum. Implementation of the correlation is done through an ad hoc assumption: $q \leq q_{cut} \rightarrow \cos^{-1} \frac{\vec{x_1}\cdot\vec{x_2}}{|\vec{x_1}||\vec{x_2}|} \leq 41.4°$, i.e. the momentum cut has already restricted their spatial origins $\vec{x_1}, \vec{x_2}$ to lie within a cone of solid angle $\frac{4\pi}{8}$ from each other. In other words, the neutron must lie within a cone of solid angle $\frac{4\pi}{8}$ from the proton before the probability of the pair's passing the spatial cut is calculated. As a result of the "cone" cut, the spatial cut is applied to only a fraction (~27%) of the total proton-neutron pairs, and the probability a pair from this subset passes the r_{cut} is greater than it is for a pair from the entire set without the cone cut. Fig. 3.10 shows the probabilities for different σ_{source}, assuming the same r_{cut}=3fm.

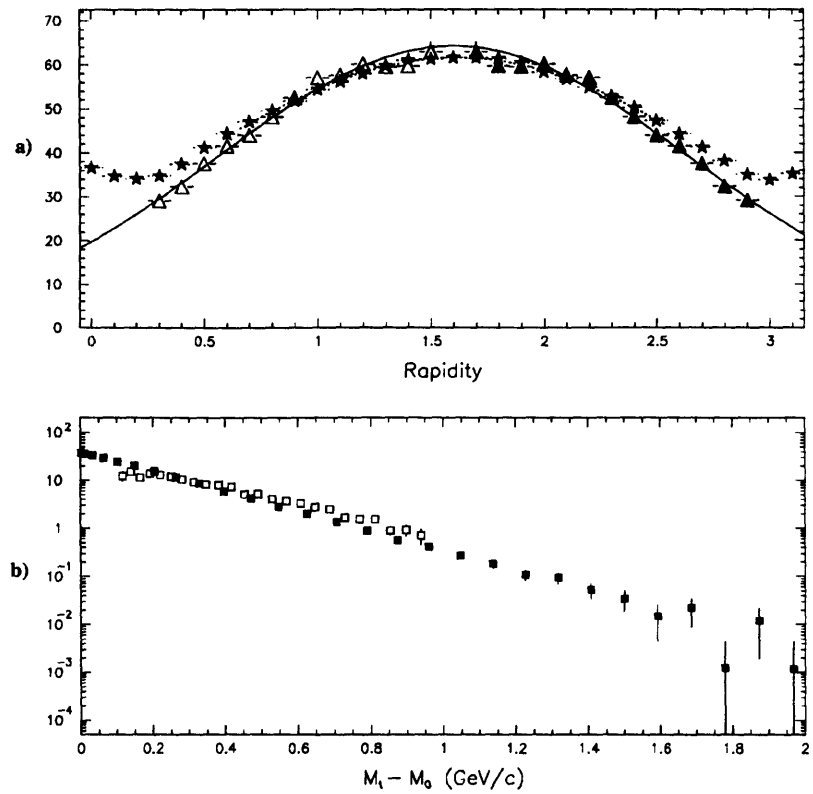

Figure 3.7: The E866 proton results and the ARC predictions. a) The proton dN/dy—E866 (triangles) and the ARC prediction (stars). b) The proton p_t distribution for the rapidity window y=[1.25,1.5]—E866 (squares) and the ARC prediction (filled-in squares).

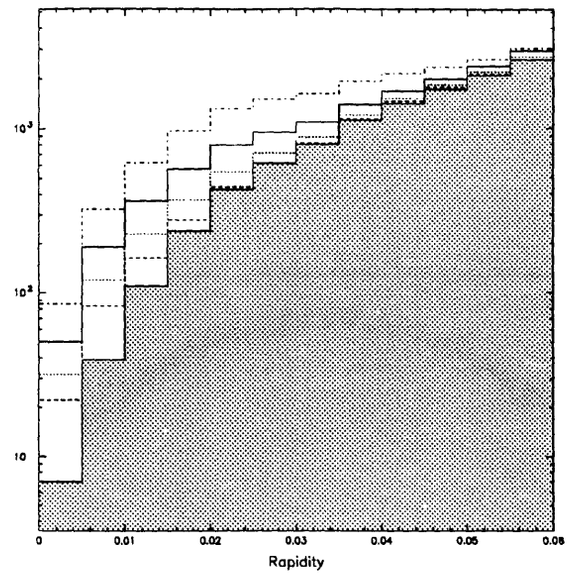

Figure 3.8: The background q-distribution calculated from ARC(hatched) and the modified distributions obtained by distorting the background with the correlation functions corresponding to σ_{source}=3 fm(dot-dash) 5 fm(solid), 7 fm(dotted), 9 fm(dash); for y=[1.25,1.5].

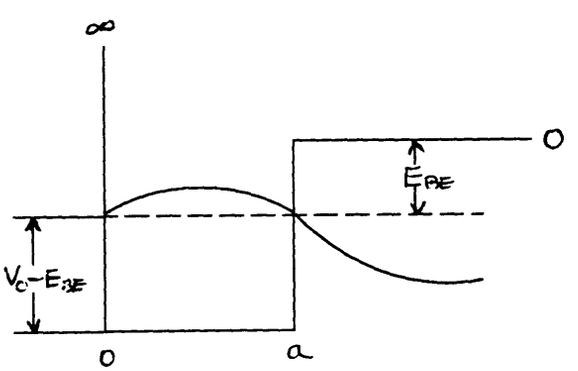

Figure 3.9: The deuteron potential well is approximated with a square well of size a and depth V_0. They are not independent, however, but related to each other through the deuteron binding energy E_{BE}. See text for detail.

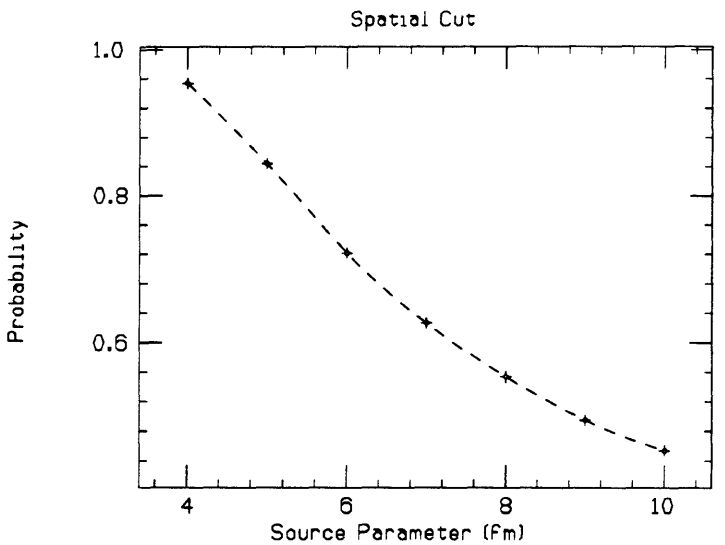

Figure 3.10: The spatial cut, or the probability that a p-n pair has the spatial separation less than r_{cut}=3fm, when the σ_{source}=3-10 fm and the *cone* cut is set at $\frac{4\pi}{8}$. See text for discussion.

Chapter 4

Discussion

4.1 Integrated Yield, dN/dy

It is of great interest whether the deuteron dN/dy can tell us something about the source the way proton-proton interferometry can. To date, the only method of extracting information about the source from the deuterons is by assuming thermal equilibrium. But by treating the deuterons in a way analogous to the p-p correlation, the source parameter can be measured independent of the thermodynamic status of the source. Both p-p interferometry and the new way of measuring the source with the deuteron dN/dy rely on the existence of the attractive strong force which enhances the probability of finding nucleon pairs with small relative momentum q. Whereas in proton interferometry one obtains a q-distribution that is compared with the theoretical prediction to extract the source parameter, with the deuterons one only has the integrated yields, dN/dy, to work with. Because a "number" is a much less restrictive observable than a "distribution", there is a larger uncertainty in such a measurement. But this is an inherent difficulty in studying cluster production and comes from the fact that the relative momentum information gets lost when a stable cluster is formed. One can minimize the uncertainty by making sure other sources of uncertainty are properly understood, and by emphasizing the *difference* between the predictions with and without the p-n correlation rather than the absolute yield of either prediction. On the other hand, when the q_{cut} and r_{cut} are more reliably implemented by convoluting the deuteron wave function to q and Δr, then one should be able to say something more definitive about

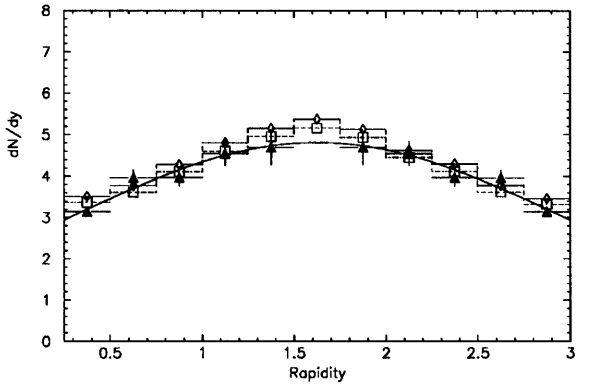

Figure 4.1: The E866 deuteron results (filled-in triangles) and the ARC predictions with (diamonds) and without (squares) the momentum correlation. σ_{source}=8 fm. q_{cut}=60 MeV/c.

the source, by measuring the deuteron dN/dy.

Our greatest uncertainty comes from ignoring the deuteron wave function and picking q_{cut} and r_{cut} somewhat arbitrarily. The amount of enhancement in dN/dy from the p-n momentum correlation depends on q_{cut}, for the correlation function approaches one for large q and the number of pairs is a very steeply rising function of q. So, for a large q_{cut}, any enhancement present at low q is obscured by numerous other pairs at large q. Another source of uncertainty is the dynamical correlation. This effect, as was mentioned previously in Section 3.7, is due to the preferential emission of particles at a normal angle from the source surface. It is also the cause of uncertainty in interferometry, where one believes the actual source size is greater than a measured value, because the dynamical correlation allows one to observe only a fraction of the total volume.

The predictions are made In Fig. 4.1 is plotted the measured deuteron dN/dy and the

ARC prediction using σ_{source}=8 fm and q_{cut}=60 MeV/c for correlated and uncorrelated dN/dy. The difference between the two is about 10% throughout the rapidity range. The value of 8 fm was chosen by comparing the predictions for radii 3-9 fm in the increment of 1 fm with the data and seeing which radius gives the best prediction. In order to see if 8 fm is a reasonable value for σ_{source}, we convert σ_{source} to the RMS of the source by multiplying it with $\sqrt{\frac{3}{2}}$ to obtain 9.8 fm. As a reference, the impact parameter averaged number of participants in the central 8.2% of inelastic collisions is about 325, (see Appendix B.) which gives an RMS radius of 6.2 $fm = 0.82 \times (325)^{1/3} + 0.58$ fm at normal nuclear density [Vut92]. We expect the measured radius to be larger than the radius deduced from the number of the participant baryons because in a collision there are also a large number of produced pions as well as the nucleons populating the collision region. Yet, it is still difficult to decide what these numbers really mean due to the assumptions that went into the prediction. Despite uncertainties in the input as well as possible multiple interpretations of the output, the crude study presented here hints at a potential application of the deuteron dN/dy to measure the source parameter.

To test the dependence of σ_{source} on q_{cut}, the deuteron dN/dy is plotted in Fig. 4.2 once more, but this time with q_{cut}=45MeV/c. The value of 45 MeV/c is chosen based on a slightly different physics argument. When a deuteron is excited with energy greater than its binding energy, E_{BE}, it dissociates into a proton and a neutron. The minimum energy required for dissociation is then E_{BE}, which is shared equally by the proton and the neutron. So

$$E_{BE} = 2 \cdot \frac{q_{cut}^2}{2m} \quad , \quad q_{cut} = \sqrt{E_{BE} \cdot m} = 45\text{MeV/c} \tag{4.1}$$

Here, the inclusion of the strong interaction has a more pronounced effect on the deuteron dN/dy. Without the low-q enhancement one already predicts too few deuterons after the momentum cut alone, but σ_{source}=5 fm gives a reasonable fit to the data if the low-q enhancement is included.

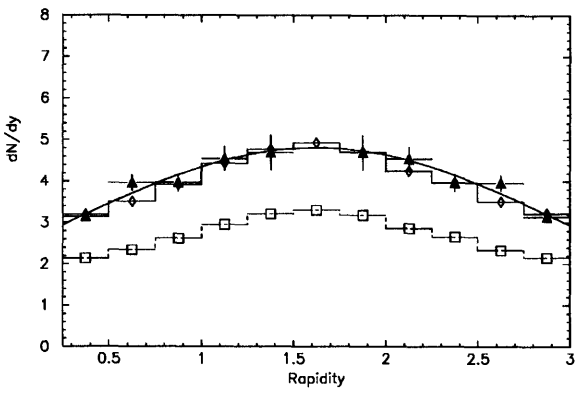

Figure 4.2: The E866 deuteron results (filled-in triangles) and the ARC predictions with (diamonds) and without (squares) the momentum correlation. σ_{source}=5 fm. q_{cut}=45 MeV/c.

4.2 P_t Distribution

The Coalescence Model is often criticized for predicting the same inverse slope of the transverse momentum distribution (often refered to as *temperature*) for the deuterons and the protons. This is in disagreement with the observation (See Par92 for Si+Au; and Fig. 4.3 for Au+Au) that the deuteron "temperature" is larger by 50 MeV or more throughout most of the rapidity. The deuterons produced through coalescence should have exactly the same inverse slope as the protons in the limit $q_{cut} \rightarrow 0$. For a finite q_{cut}* the transverse momentum distribution of the deuterons deviates from the strict exponential in m_t and fitting it to m_t gives an effective temperature that is at most a few percent larger than the proton temperature. Therefore, this by itself is insufficient to explain the observed large difference

*Appendix C describes how the proton p_t spectrum can be numerically integrated to produce the deuteron p_t spectrum.

between the two temperatures. Appendix B describes the procedure of numerically deriving the deuteron p_t spectrum starting from the proton p_t spectrum. As shown in Fig. 4.3, the low-q enhancement has little effect on the deuteron slope.

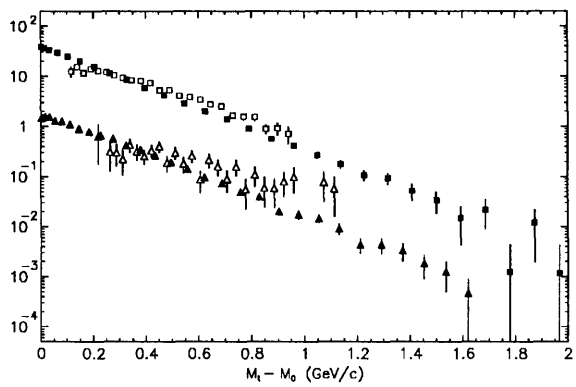

Figure 4.3: The transverse momentum distributions for the protons (squares) and the deuterons (triangles) in the rapidity bin [1.25, 1.5]. Empty symbols are the data and filled-in symbols are the ARC predictions. σ_{source}=8 fm.

However, a hypothesis which might explain this difference is that of an expanding *fireball*—the name often ascribed to the hot and dense nuclear matter formed in the central rapidity region following the heavy ion collision. In this picture, the compressed matter collectively expands with velocity $\vec{v}_0 = v_0\hat{r}$, boosting all particles' outward velocities by the same amount (non-relativistically speaking). Consequently, the particles appear to be coming from a "hotter" source. By the equipartition function, a particle that is at thermal equilibrium with the environment at temperature T_0 has an average kinetic energy of $\frac{1}{2}k_BT_0$ for each degree of freedom it possesses. Then a particle at a given rapidity has the average transverse kinetic energy that is equal to the temperature, i.e. $T_0 = \frac{1}{2}m(v_x^2 + v_y^2) = \frac{1}{2}mv_t^2$, for it has now

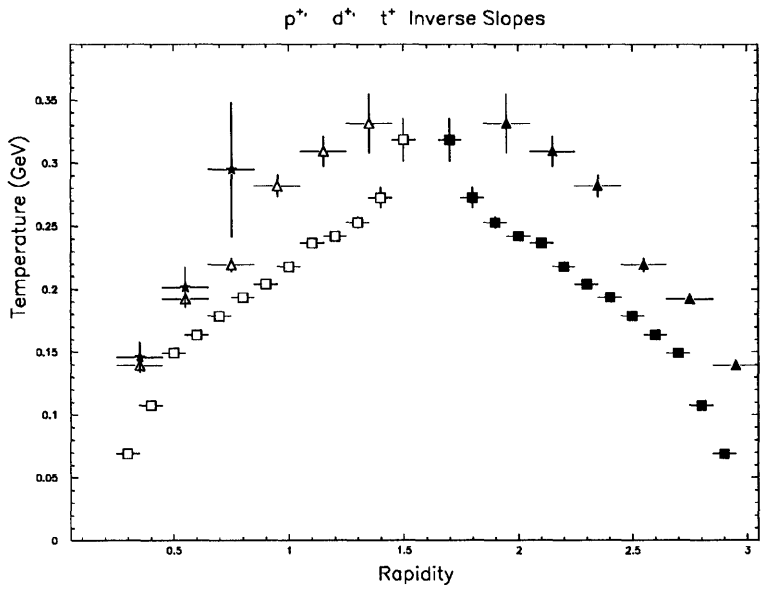

Figure 4.4: The proton (squares) , deuteron (triangles), and triton (stars) temperatures for the central 30% of the cross-section.

two degrees of freedom. On the other hand, the effective temperature when the particle's velocity and the collective expansion velocity are taken together is $T_{eff} = \frac{1}{2}m(v_t + v_0)^2$. So the difference between the original temperature and the new effective temperature is $\Delta T = T_{eff} - T_0 = v_0\sqrt{2T_0 m} + \frac{1}{2}mv_0^2$, which is greater for heavier particles. Fig. 4.4 shows the temperatures of the p, d, and t from the most central 30% of the inelastic events. Because of the large error bars for the tritons, one cannot tell from the plot whether the tritons indeed have a larger inverse slope than the deuterons at mid-rapidity. If it can be shown that $T_t > T_d > T_p$ at mid-rapidity, then it will be strong evidence for the collective transverse expansion.

Chapter 5

Conclusion

In central Au+Au collisions, close to 10% of the participant protons at mid-rapidity leave the collision region bound inside the deuterons. Despite the strong momentum correlation that must exist between the protons and the neutrons emitted from the fireball, the existence of the bound state and the difficulty of experimentally observing unbound neutrons make it impractical to determine the correlation function directly from the actual distribution of the relative momentum.

As the first step to understand the role of the proton-neutron correlation in deuteron production, this thesis applied the proton-neutron correlation function to the ARC output, in the context of the identical particle interferometry. Subsequent coalescence in phase space gives a prediction for the deuteron dN/dy to be compared with the data. Because the proton-neutron correlation function is a function of the source size, this method allows the measurement of the source size without assuming thermal equilibrium. This is different from the Sudden Approximation Model, where such an assumption is required in order to associate the deuteron yields with the source volume.

As we saw, the low-q enhancement can result in a deuteron dN/dy that is twice as large as the unenhanced dN/dy, for $q_{cut} \simeq 45$MeV/c. For a larger q_{cut}, the correction to dN/dy becomes smaller, being about 10% for q_{cut}=60MeV/c. The measured σ_{source}'s are about 5 fm and 8 fm for the q_{cut}=45MeV/c and 60MeV/c, respectively, by fitting the predictions to the data, but a more quantitative discussion is not warranted at this point because of

the crude approximations that went into applying the momentum and spatial cuts as well as implementing the dynamical correlation. But that should not be a reason to think the whole concept of extracting the source size based on the deuteron dN/dy is an untenable dream. Quite the contrary, one should view it as an encouragement to do a more precise calculation, since such crude approximations as made here give a very reasonable answer.

An important observation that can be made from the study is that apart from its potential usefulness in measuring the source size, the low-q enhancement for the proton-neutron pairs can appreciably increase the number of deuterons over the statistically expected value. Thus, in order to predict the deuteron dN/dy correctly, one has to include the low-q enhancement in the calculation. This is not feasible with most of the phenomenological models for the nuclear collision, e.g. ARC which does not parameterize the nucleon-nucleon potential function to predict the momentum dependent enhancement. By definition, such models give the background q-distribution for the p-n pairs. The use of the correlation function is an easy way to obtain the actual distribution by knowing only the background distribution, and hence allows an accurate prediction of the deuteron yield once the coalescence momentum and spatial cuts are determined from the deuteron wave function. It is, therefore, erroneous to try to fit the yields by raising the momentum cut, while ignoring the low-q enhancement that can change the yields substantially.

The study shows that the transverse momentum distribution of the deuterons which ARC fails to reproduce cannot be explained by low-q enhancement. Even if the ARC prediction of the proton p_t distribution were correct, it still does not change the conclusion that the predicted deuteron temperature should be very near the predicted proton temperature. The observed proton temperature is greater than the predicted proton and deuteron temperatures and the deuteron temperature is even greater than the observed proton temperature. At present there is no definitive explanation, although collective expansion may be the answer.

Though the thesis is focused on the deuterons, heavier clusters should not be neglected, for they contain valuable information not available in the deuterons. Heavy clusters, first

of all, provide additional constraints on coalescence-based models attempting to explain cluster production statistically. If, for instance, cluster production depends solely on the statistical probability of finding nucleons close to each other in phase space, then the ratio $R_{td} = (\frac{dN}{dy})_t/(\frac{dN}{dy})_d$ should closely resemble the ratio $R_{dp} = (\frac{dN}{dy})_d/(\frac{dN}{dy})_p$. These ratios are plotted in Fig. 5.1 for the central-30% events by fitting the p,d,t dN/dy's with polynomials of order 4, 0, and 3, respectively, and taking the appropriate ratios. The vertical lines in Fig. 5.1(d) indicate the rapidity coverage available for the deuterons and the tritons. Both ratios are about 10% near the target rapidities and have a similar overall shape. However, the extrapolations toward the mid-rapidity seem to deviate from each other. This may be due to the large contribution to the triton yields from the target fragmentation, which distorts the fit to the triton dN/dy and predicts fewer tritons at mid-y. A greater rapidity coverage for the tritons is necessary to answer whether the ratios actually diverge as the extrapolations show, or converge as expected according to the coalescence model.

One evidence that nuclear fragmention is a principal mode of heavy cluster production in the target rapidity region comes from the the integrated yield spectra of the tritons for various centrality cuts. Data show the shape of the dN/dy distribution is almost independent of the centrality of the collision, indicating their production mechanicm is similar for all centralities. See Fig. 5.2.

Heavy-ion physics is not new but *relativistic* heavy ion physics *is*. Relatively little effort has been made until now to understand cluster production in nuclear collisions at the AGS energies. Current approaches to understand it are mostly statistical and phenomenological. A difficulty in studying cluster production starting from the first principles is that in order to understand it thoroughly one must have detailed knowledge of the soft strong interaction, which itself is one of the goals of heavy-ion physics. Though there are uncertainties and complications arising from low-energy effects such as fragmentation, one can learn much by studying cluster production at the AGS energies. An example given in this thesis is the effect of the momentum correlation in deuteron production, which may supplement

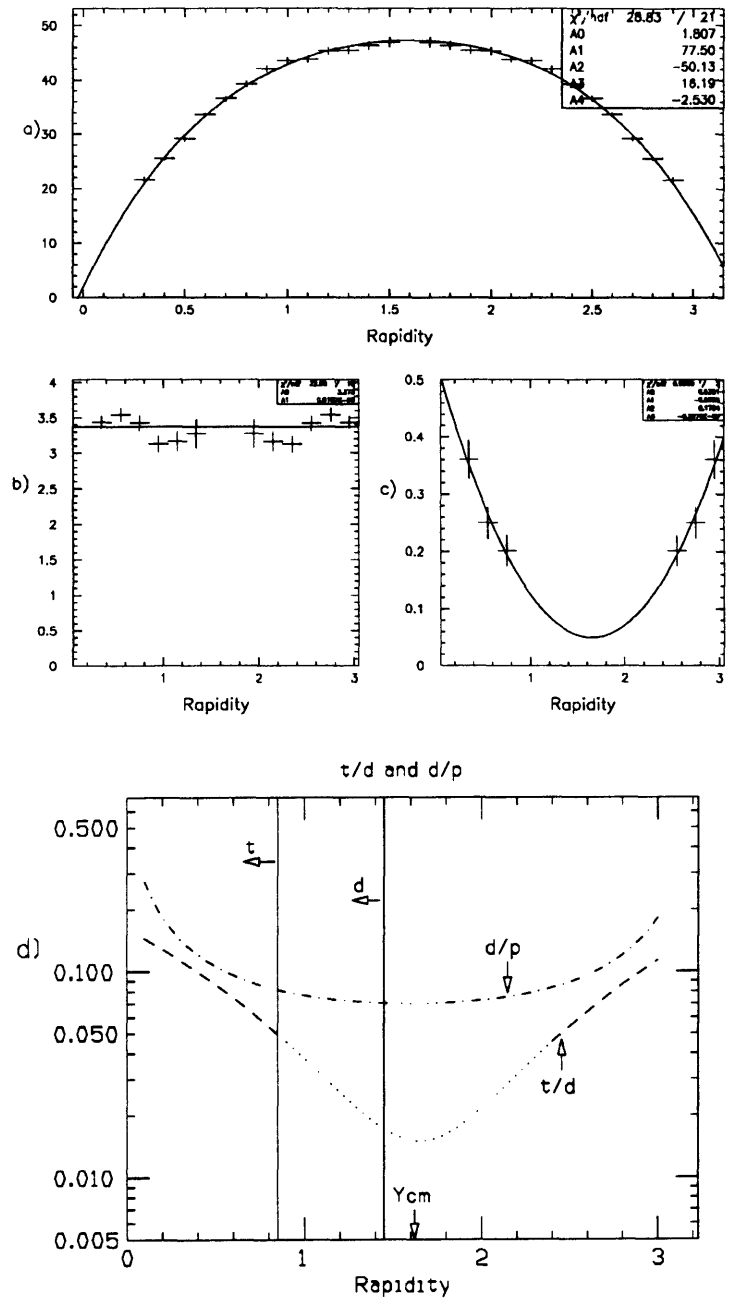

Figure 5.1: The integrated yields of a) p, b) d, c) t for the central 30% of the inelastic collisions, and d) the ratios, R_{dp} and R_{td}. The dotted portions correspond to the extrapolations based on the measured yields in the rapidity ranges indicated by the solid vertical lines.

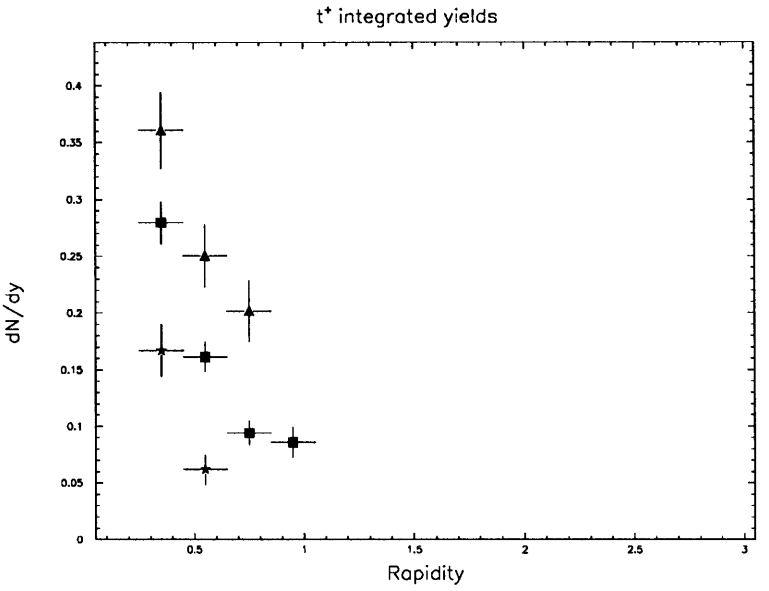

Figure 5.2: The triton integrated yields for three different centrality cuts: The central 30% (triangles), the peripheral 50% (stars), and the minimum bias (squares).

and/or complement proton interferometry, and may provide an independent measurement of the source distribution. A more realistic calculation could reveal if the deuteron dN/dy is sensitive enough to tell the difference of a fraction of a fermi in source size, which is the present precision for the proton-proton correlation measuments.

Appendix A

Particle Spectra

In this appendix, the transverse momentum distributions for $p, d, t, {}^3\mathrm{He}$ in the Au+Au collisions are presented. Summarized after the p_t spectra for each particle species are their integrated yields as well as the inverse slope parameters. In fitting the p_t distributions, the exponential in $m_t = \sqrt{p_t^2 + m^2}$ is assumed. The transverse momentum spectra are presented for three different centrality cuts. Central Events are defined as the most central 8.2% of the total cross-section measured by the ZCAL for p and d, but the central 30% for t and ^{3}He. These choices are, of course, motivated by the available statistics, but otherwise arbitrary. 8.2% is chosen since the corresponding impact parameter is ~ 4 fm, which was used to generate the simulated events. Peripheral Events mean the most peripheral 50% of the cross section for all particle species. Finally, the particle spectra from the Minimum Bias events are plotted. In all p_t spectra, the vertical scale is $E\frac{d^3N}{dp^3}[GeV/c]^{-2}$, which is the invariant cross section, also written as $dN/(2\pi p_t dp_t dy)$.

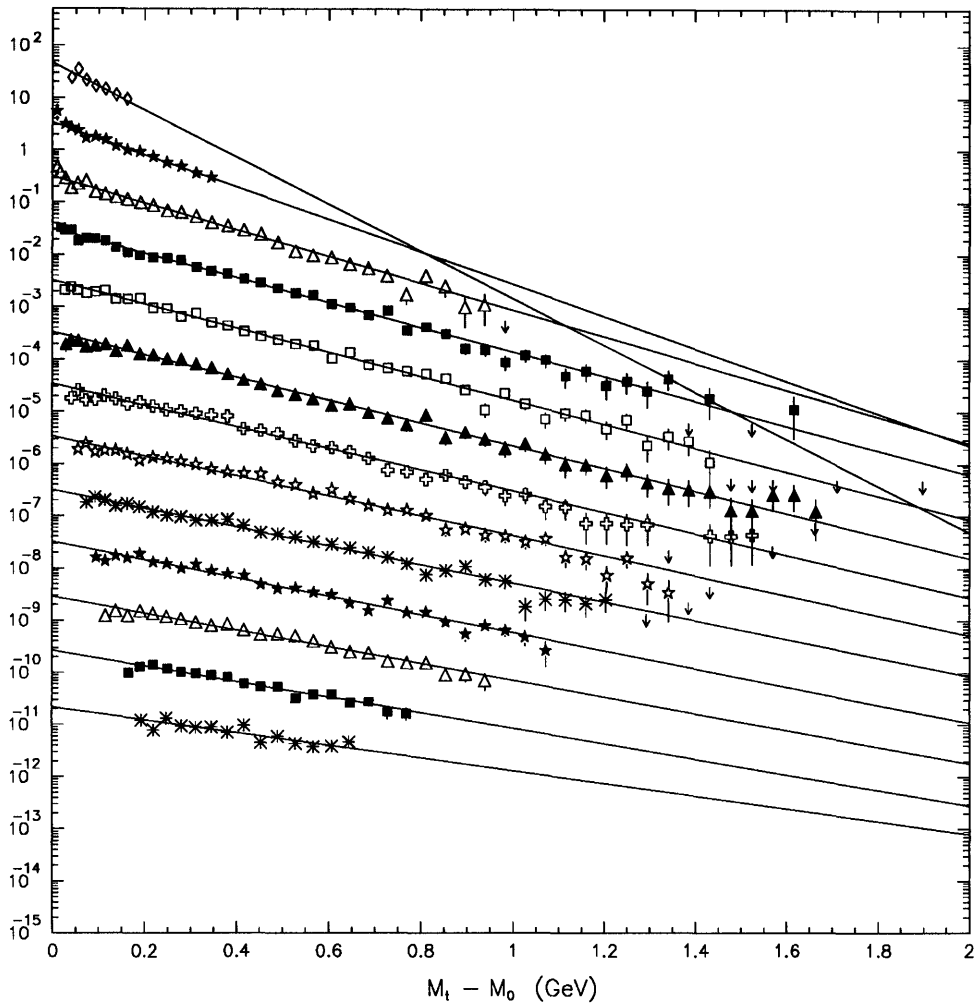

Figure A.1: The proton p_t spectra for the Central(8.2%) events. Each spectrum corresponds to a rapidity window, starting from [.25,.35] at the top to [1.45,1.55] at the bottom. Each successive slice has been scaled down by a factor 10 relative to the one before.

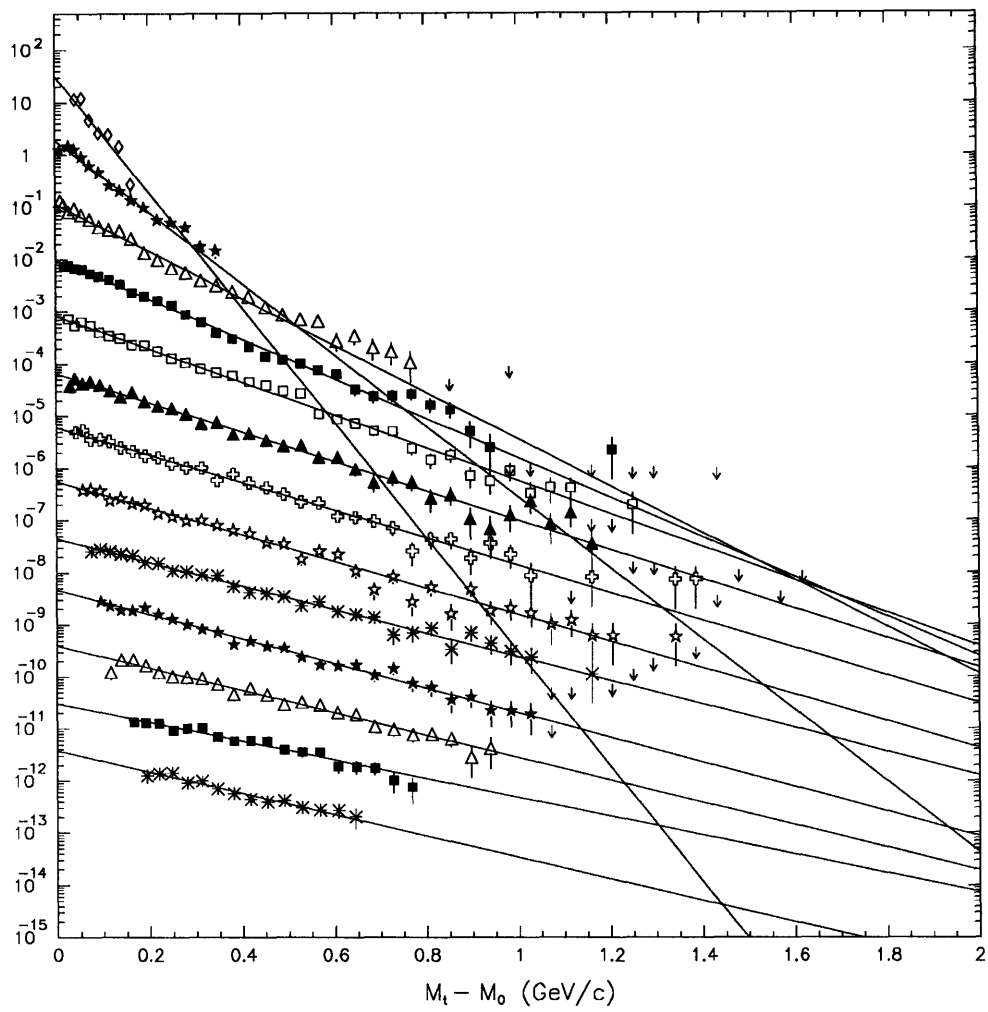

Figure A.2: The proton p_t spectra for the Peripheral(50%) events. Each spectrum corresponds to a rapidity window, starting from [.25,.35] at the top to [1.45,1.55] at the bottom. Each successive slice has been scaled down by a factor 10 relative to the one before.

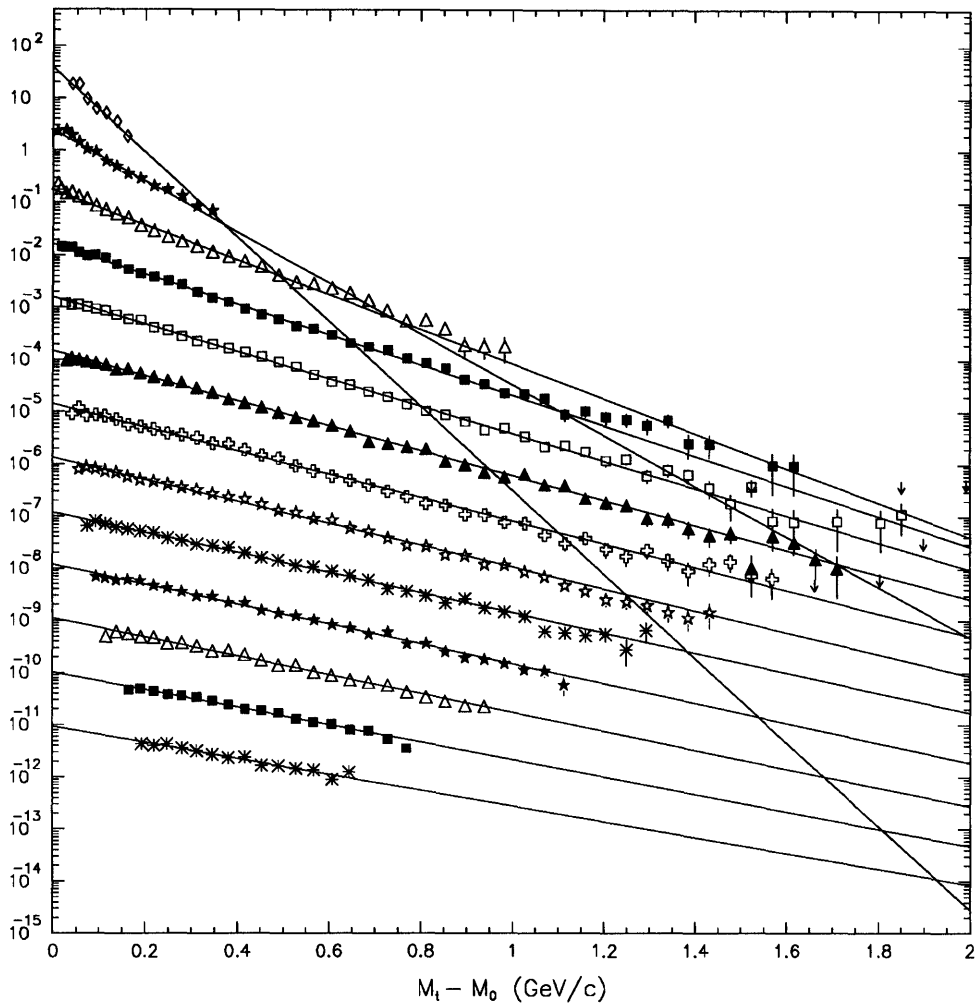

Figure A.3: The proton p_t spectra for the Mininum Bias events. Each spectrum corresponds to a rapidity window, starting from [.25,.35] at the top to [1.45,1.55] at the bottom. Each successive slice has been scaled down by a factor 10 relative to the one before.

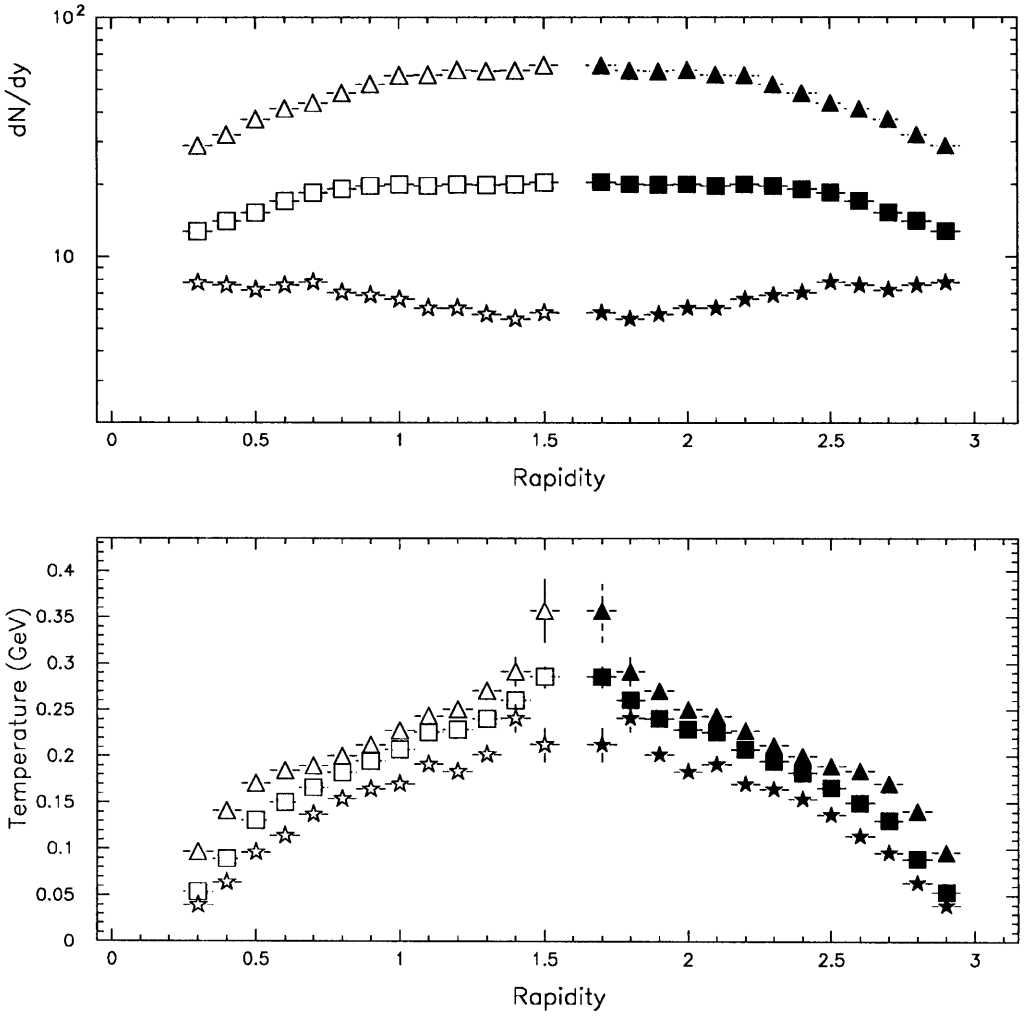

Figure A.4: (a) The proton integrated yields dN/dy for the Central (triangles), the Peripheral (stars), and the Min.Bias (squares) events; and (b) their corresponding temperatures. The filled-in symbols are reflections about y_{CM}=1.6. Because the projectile and the target are both Au, the dN/dy and T distributions in the forward rapidity region should be the same as in the backward rapidity region.

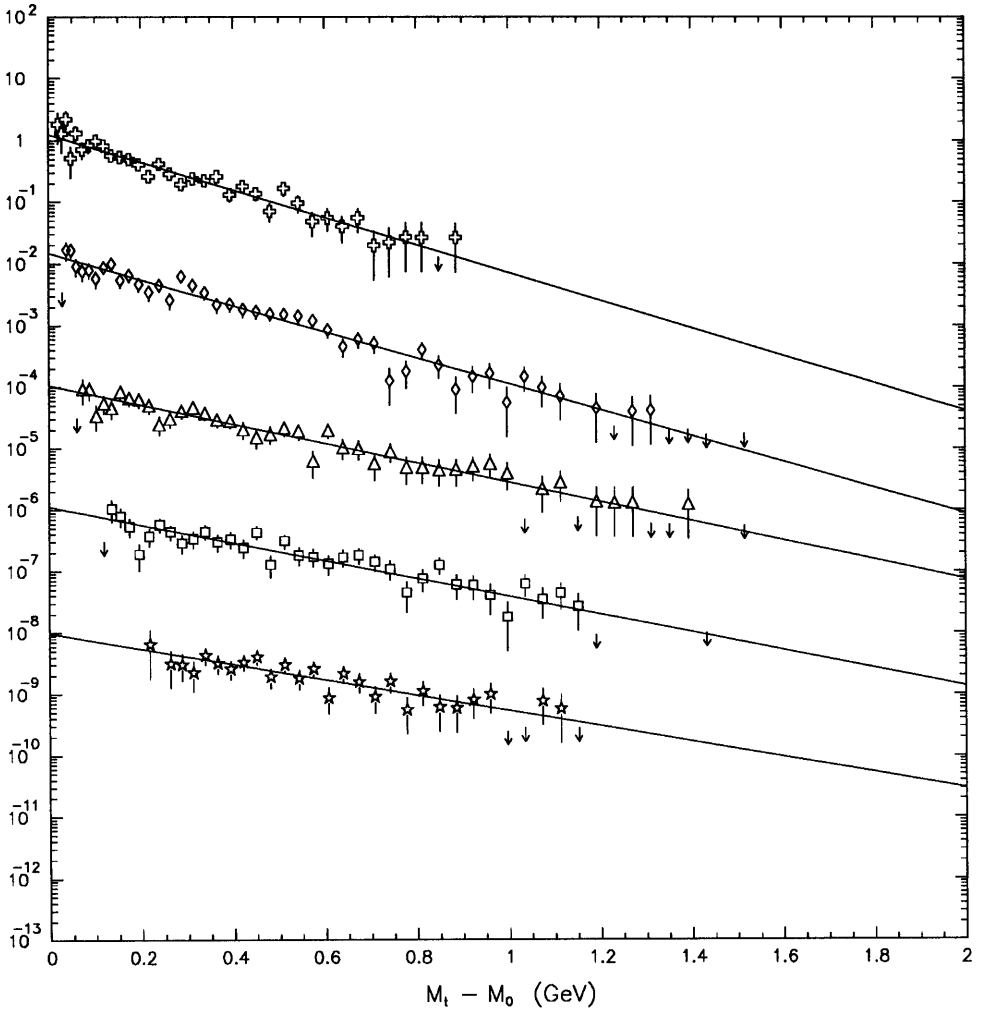

Figure A.5: The deuteron p_t spectra for the Central(8.2%) events. Each spectrum corresponds to a rapidity window, starting from [.25,.5] at the top to [1.25,1.5] at the bottom. Each successive slice has been scaled down by a factor 100 relative to the one before.

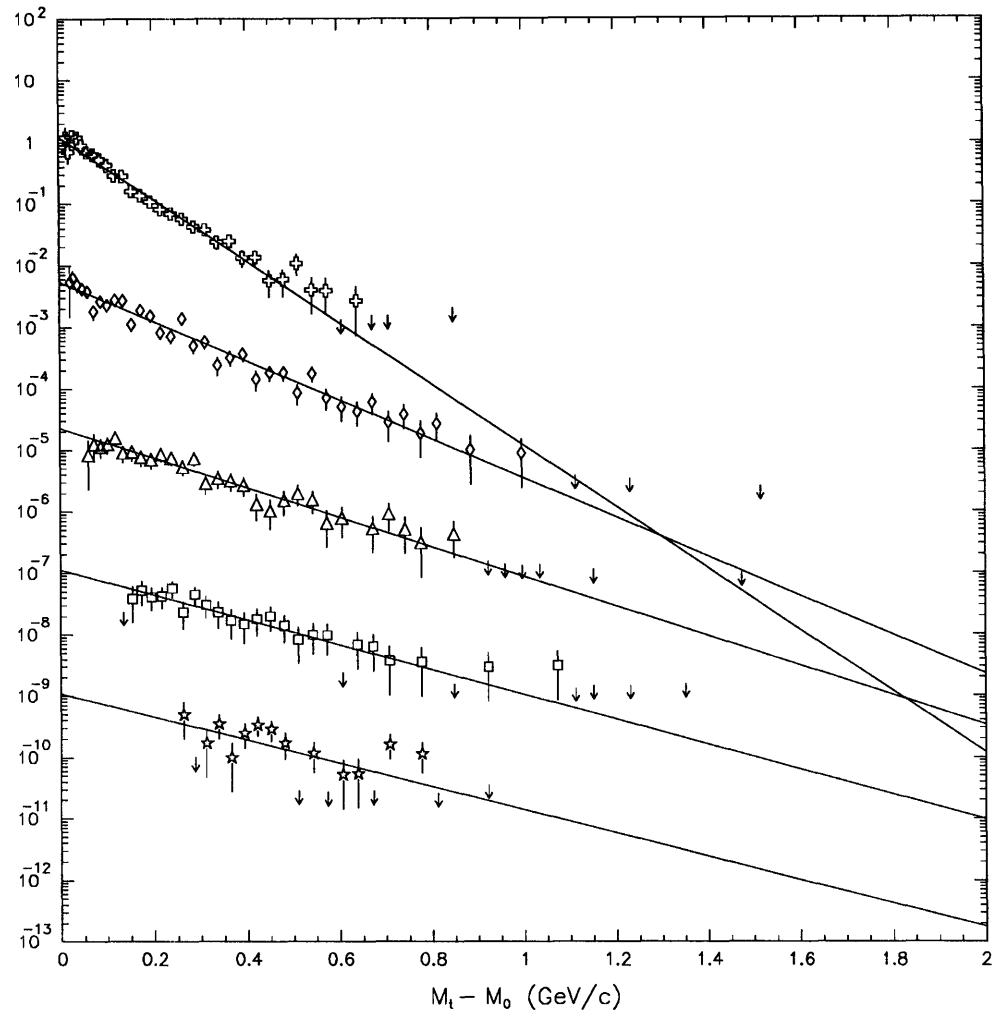

Figure A.6: The deuteron p_t spectra for the Peripheral(50%) events. Each spectrum corresponds to a rapidity window, starting from [.25,.5] at the top to [1.25,1.5] at the bottom. Each successive slice has been scaled down by a factor 100 relative to the one before.

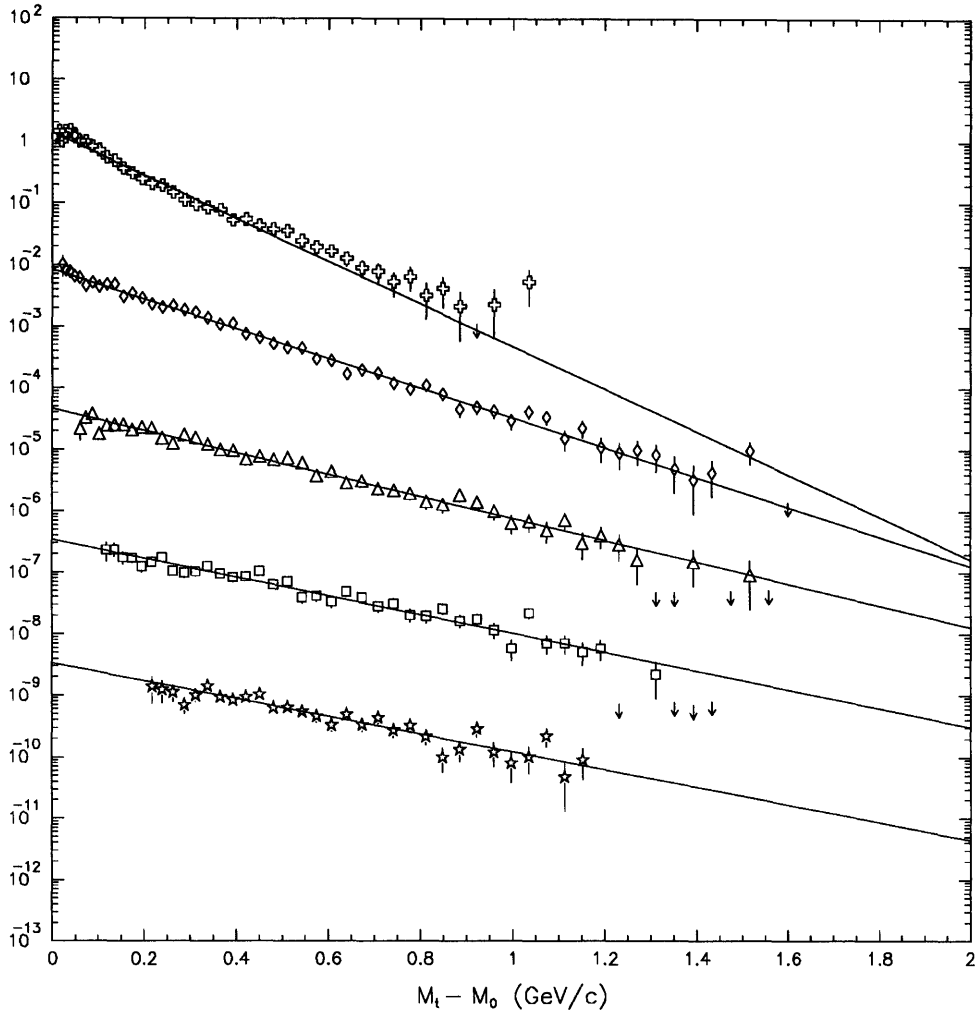

Figure A.7: The deuteron p_t spectra for the Mininum Bias events. Each spectrum corresponds to a rapidity window, starting from [.25,.5] at the top to [1.25,1.5] at the bottom. Each successive slice has been scaled down by a factor 100 relative to the one before.

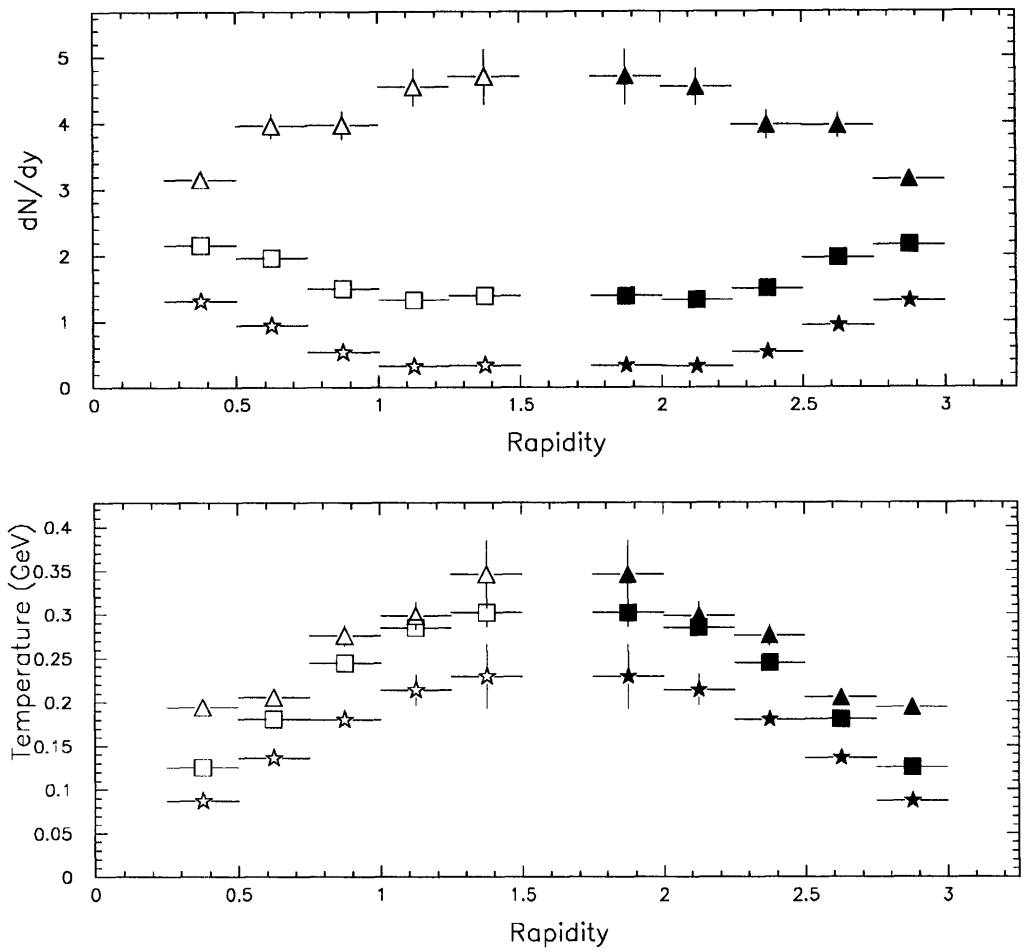

Figure A.8: (a) The deuteron integrated yields dN/dy for the Central (triangles), the Peripheral (stars), and the Min.Bias (squares) events; and (b) their corresponding temperatures. The filled-in symbols are reflections about y_{CM}=1.6.

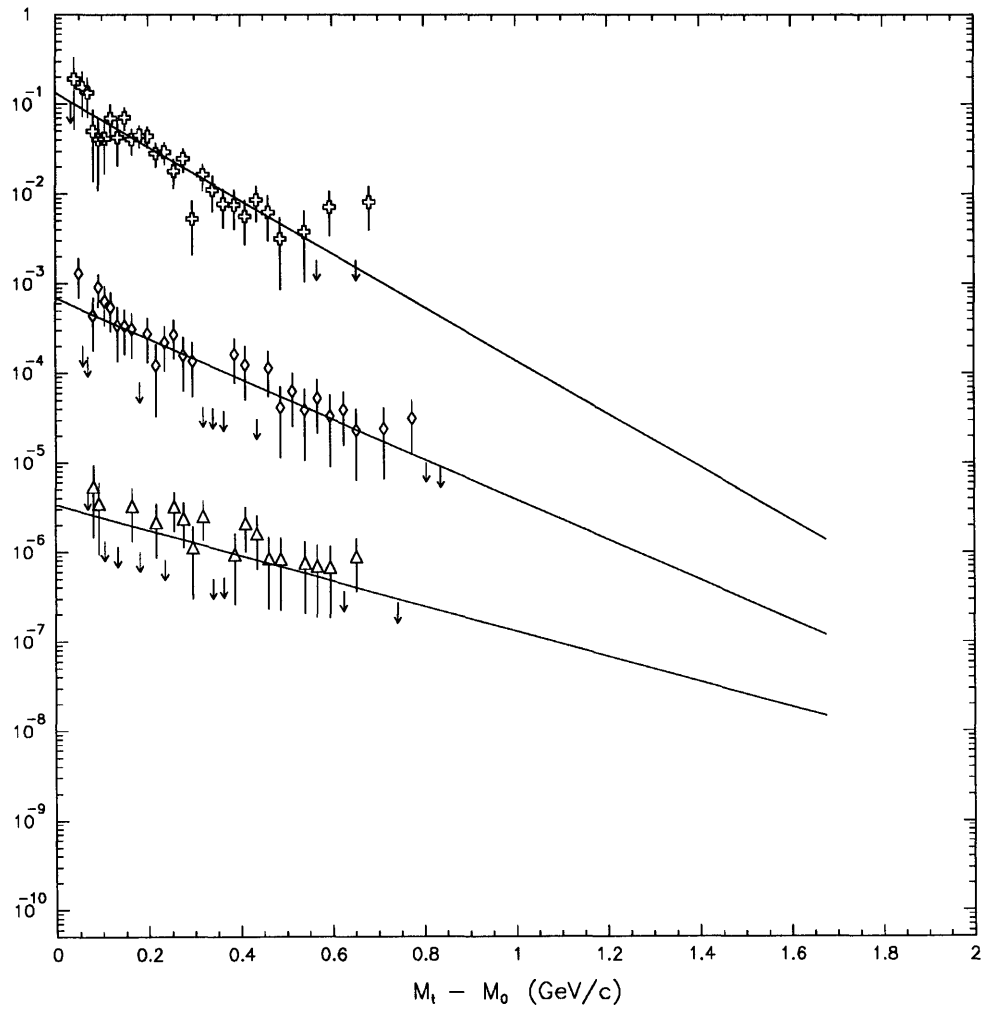

Figure A.9: The triton p_t spectra for the Central(30%) events. Each spectrum corresponds to a rapidity window, starting from [.25,.45] at the top to [.65,.85] at the bottom. Each successive slice has been scaled down by a factor 100 relative to the one before.

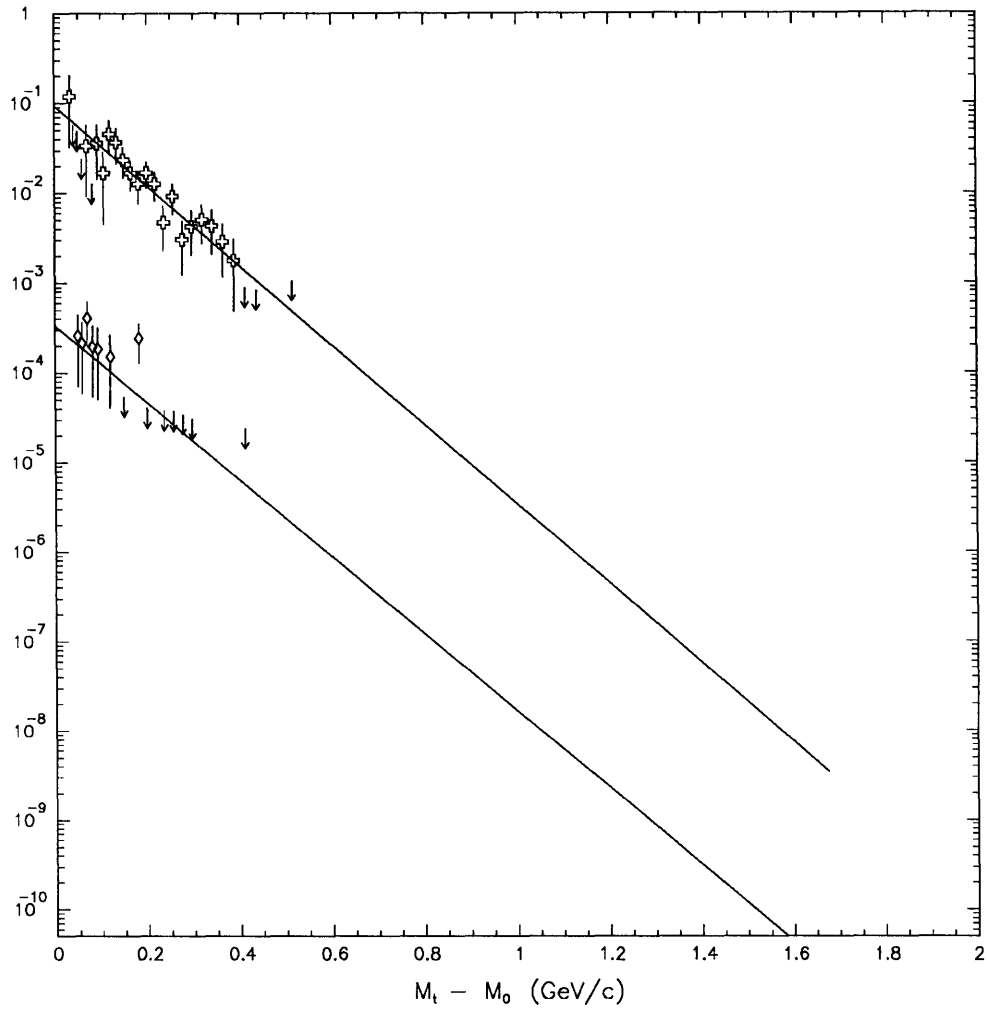

Figure A.10: The triton p_t spectra for the Peripheral(50%) events. Each spectrum corresponds to a rapidity window, starting from [.25,.45] at the top to [.45,.65] at the bottom. The second distribution has been scaled down by a factor 100 relative to the first.

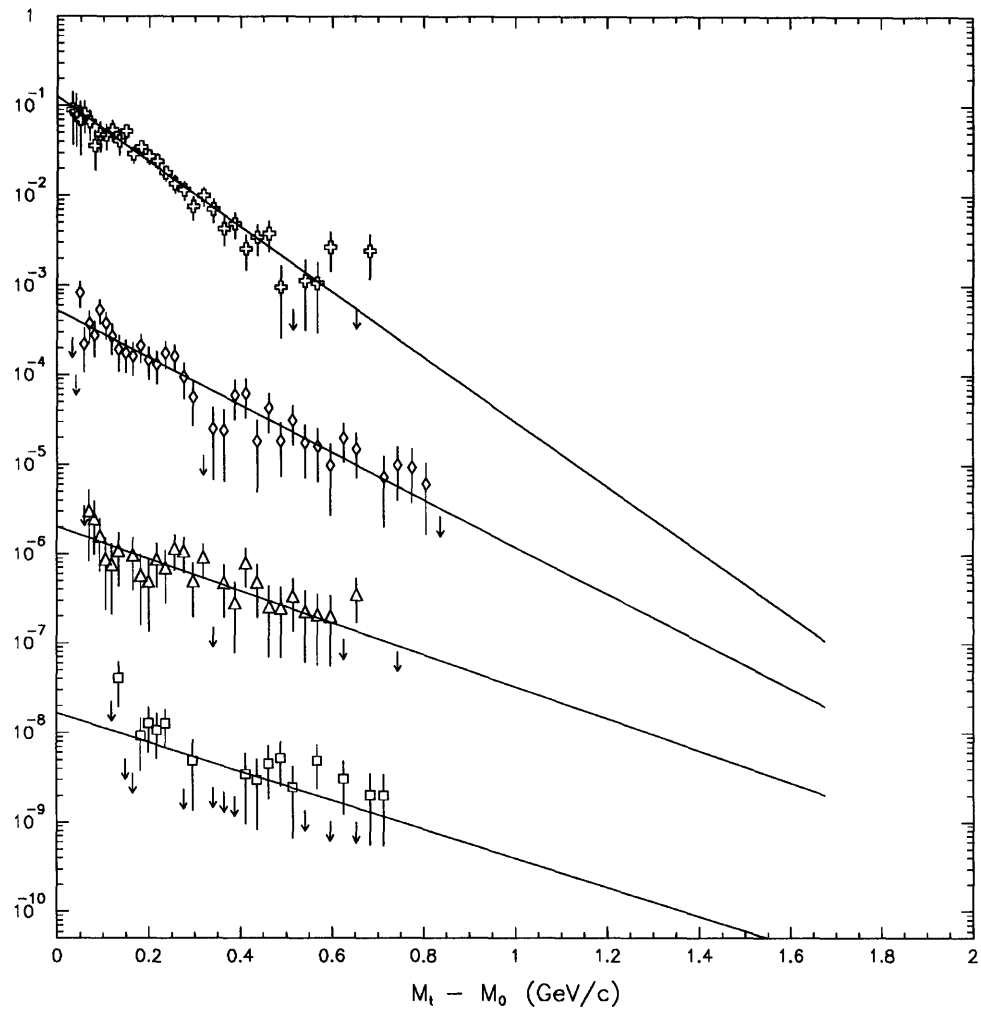

Figure A.11: The triton p_t spectra for the Mininum Bias events. Each spectrum corresponds to a rapidity window, starting from [.25,.45] at the top to [.85,1.05] at the bottom. Each successive slice has been scaled down by a factor 100 relative to the one before.

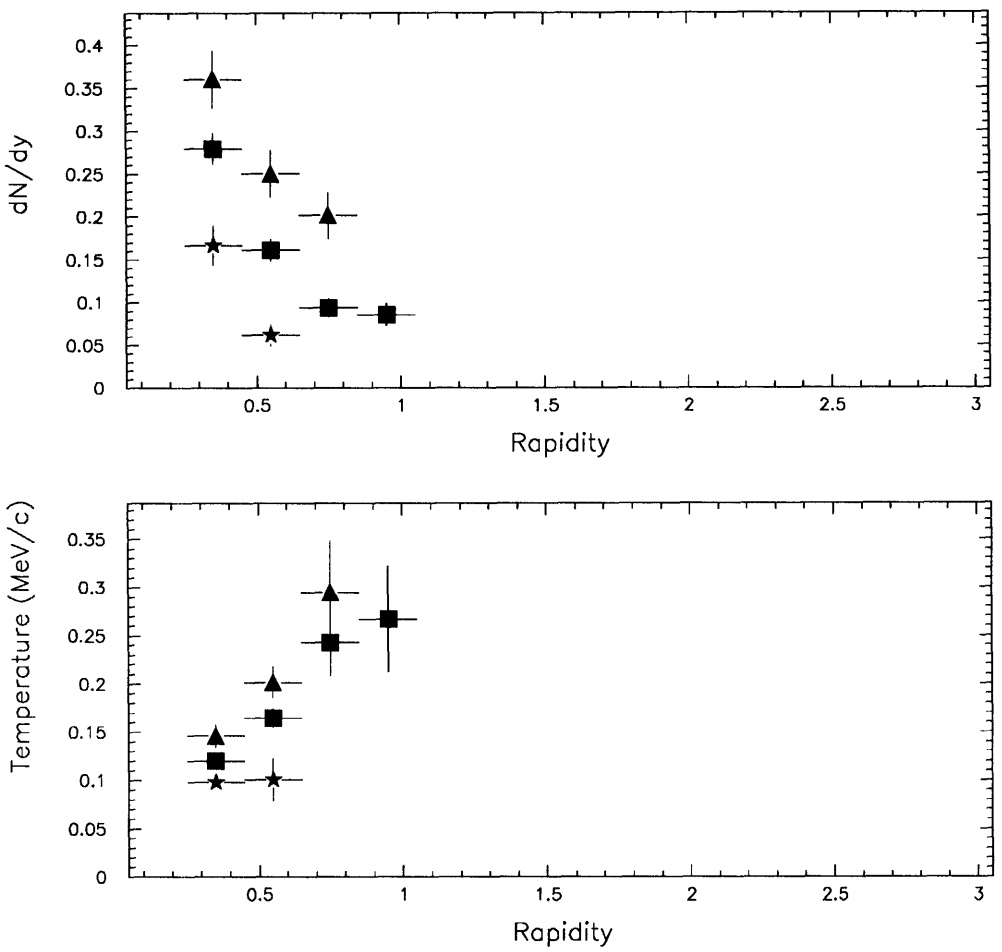

Figure A.12: (a) The triton integrated yields dN/dy for the Central (triangles), the Peripheral (stars), and the Mininum Bias (squares) events; and (b) their corresponding temperatures.

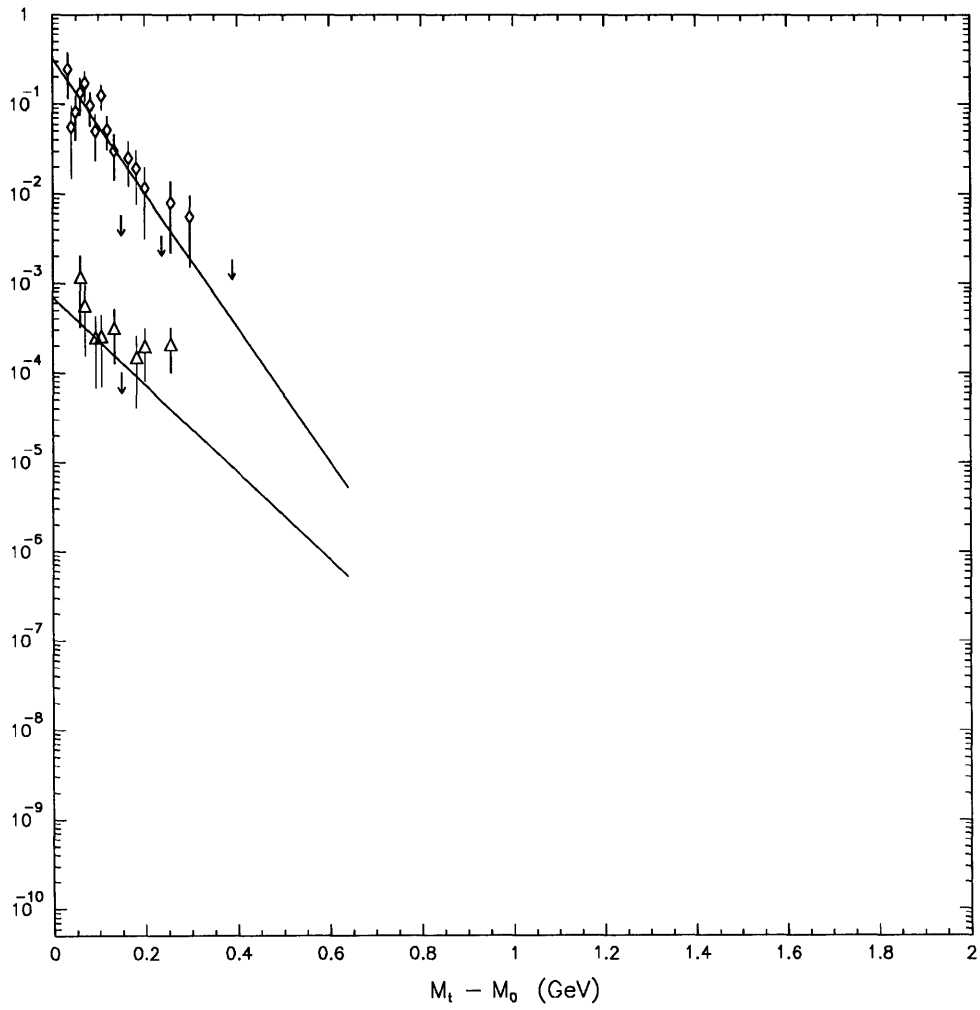

Figure A.13: The ^{3}Helium p_t spectra for the Central(30%) events. The two spectra correspond to the rapidity windows [.35,.6] at the top and [.6,.85] at the bottom. The second distribution has been scaled down by a factor 100 relative to the first.

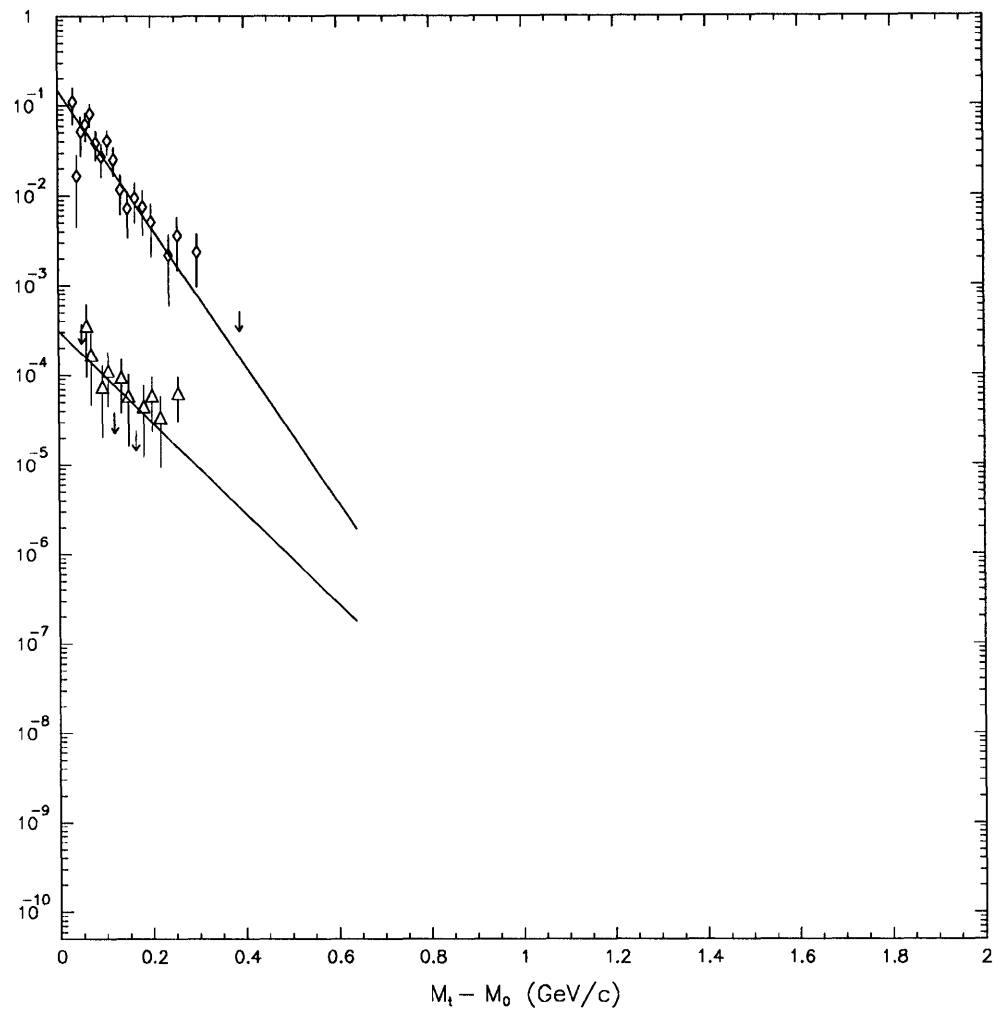

Figure A.14: The ^{3}Helium p_t spectra for the Mininum Bias events. The spectra correspond to the rapidity windows [.35,.6] at the top and [.6,.85] at the bottom. The second distribution has been scaled down by a factor 100 relative to the first.

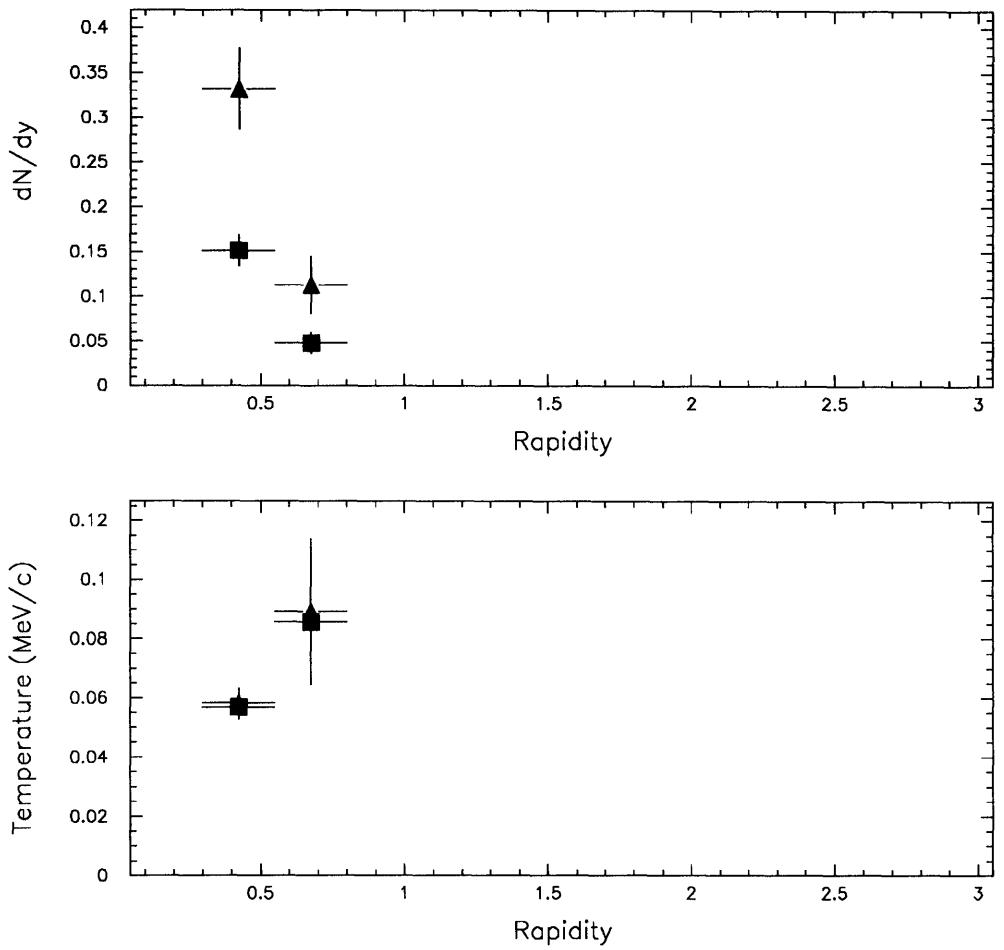

Figure A.15: (a) The ^{3}Helium integrated yields dN/dy for the Central (triangles) and the Mininum Bias (squares) events; and (b) their corresponding temperatures.

Appendix B

Number of Participants

A question that came up during the study was "What is the impact-parameter averaged number of participants in ^{197}Au+^{197}Au collisions for a given range of centrality?" One way to estimate it is to measure the energy deposited in the ZCAL and divide it by the kinetic energy of a nucleon in the projectile, i.e. $K.E. = \sqrt{p^2 + m^2} - m$=10.7GeV. Doing it this way, there is a danger of overestimating the number of spectators because there are pions produced at small angles which contribute to the ZCAL energy. An alternative method is to calculate the number, assuming clean-cut collision geometry, where the nucleons in the projectile, and only those nucleons, which lie in the direct path of the target interact, while the rest continue in the forward direction uninterrupted. This is a purely geometrical problem once we agree on the shape of the nucleus, and an algorithm was developed to compute the fractional volume of the nucleus which overlaps with the target in the collision at a given impact parameter, assuming a hard sphere of radius $R = 1.2A^{\frac{1}{3}} = 7$fm for both nuclei. This may not be the correct picture for the nuclear collisions we are looking at, because participant nucleons may interact with the spectator nucleons before they have time to leave the collision region. Nevertheless, such a calculation is useful, if not to be trusted too much, at least as a guideline in estimating the source size.

The calculation is based on figuring out the overlap volume. As far as the projectile is concerned, the target can be replaced by a cylinder of radius r_0 =7fm, whose axis is located b away from the center of the projectile as in Fig. B.1. The volume of the projectile which

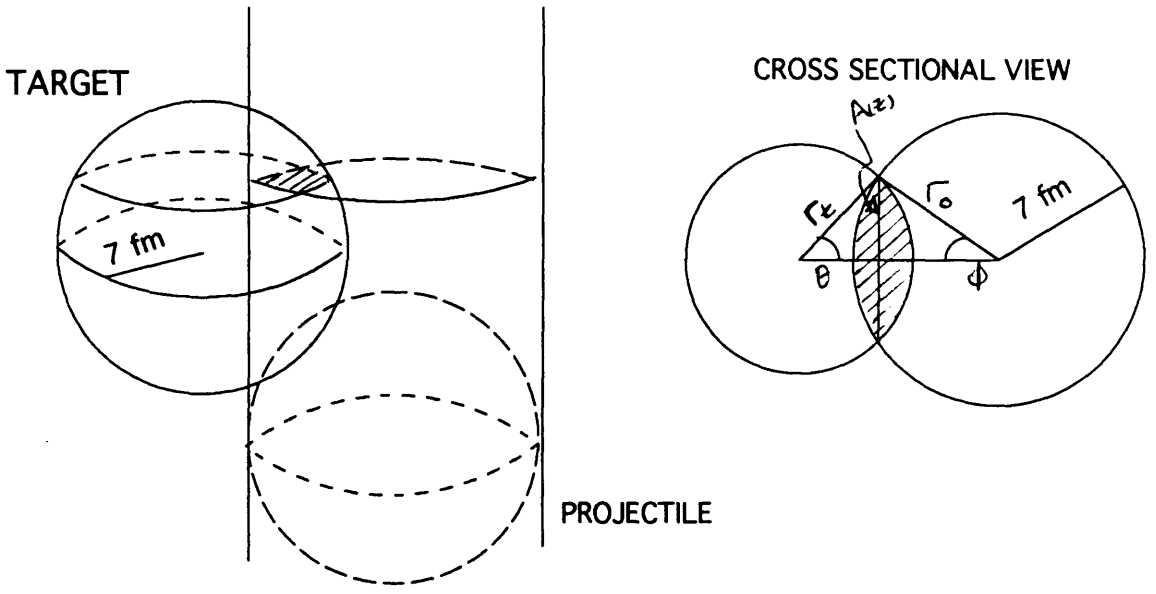

Figure B.1: The target nucleus of radius r_0 is shown. The cylinder of r_0 represents the volume swept out by the projectile as it passes by.

overlaps with the cylinder is

$$\Delta V = 2\int_0^{z_{max}} A(z)dz \tag{B.1}$$

$$\begin{aligned} A(z) &= \text{cross sectional area of the overlap at } z \\ &\quad \text{above the equatorial plane} \\ &= r_t^2\theta + r_0^2\phi - \frac{1}{2}r_t^2 \sin 2\theta - \frac{1}{2}r_0^2 \sin 2\phi \end{aligned} \tag{B.2}$$

$$\theta = \cos^{-1}\left(\frac{r_t^2 - r_0^2 + b^2}{2r_t b}\right)$$

$$\phi = \cos^{-1}\left(\frac{r_0^2 - r_t^2 + b^2}{2r_0 b}\right)$$

$$z_{max} = \begin{cases} r_0 & \text{if } b \le r_0 \\ b\sqrt{\frac{2r_0}{b} - 1} & \text{if } b > r_0 \end{cases}$$

$$r_t = \sqrt{r_0^2 - z^2}$$

The fractional volume which participates in a collision is $f(b) = \Delta V/(4\pi/3)r_0^3$, and the impact parameter averaged number of participants is

$$< N >_b = 2N_A < f >_b = 2N_A \frac{\int_{b_{min}}^{b_{max}} f(r)2\pi r dr}{\int_{b_{min}}^{b_{max}} 2\pi r dr}. \tag{B.3}$$

For the central 8.2% of inelastic events in $^{197}Au+^{197}Au$ collisions, the average number of participants $< N >_b = 325$, which corresponds to a radius of 8.3 fm.

Appendix C

Coalescence Equation

In the following is shown the equation that predicts the deuteron p_t distribution from the proton and neutron p_t distributions. Assuming the same temperature T_0 for both, we have

$$\rho(\vec{p}_{t,p}) \sim \exp^{-m_t/T_0} = \exp(-\sqrt{p_{t,p}^2 + m^2}/T_0) \tag{C.1}$$

$$\rho(\vec{p}_{t,n}) \sim \exp^{-m_t/T_0} = \exp(-\sqrt{p_{t,n}^2 + m^2}/T_0),$$

where $p_t = |\vec{p}_t|$. Then the distribution for the deuteron is

$$\rho(\vec{p}_3) \sim \int\int \rho(\vec{p}_1)\rho(\vec{p}_2)\delta^2(\vec{p}_3 - (\vec{p}_1 + \vec{p}_2) \times \Theta(q_{cut} - |\vec{p}_1 - \vec{p}_2|)\, d^2p_1 d^2p_2 \tag{C.2}$$

$$\rho(\vec{p}_3) \sim \int_\Omega \exp(-\sqrt{p_1^2 + m^2}/T_0) \exp(-\sqrt{p_1^2 + m^2 + p_3^2 - 2p_1p_3\cos\phi}/T_0) \times \Theta(q_{cut} - |2\vec{p}_1 - \vec{p}_3|)\, 2d\phi dp_1 \tag{C.3}$$

$$\Theta(a - x) = \begin{cases} 1 & \text{if } a > x \\ 0 & \text{if } a < x \end{cases}$$

$$\cos\phi = \frac{\vec{p}_1 \cdot \vec{p}_3}{|\vec{p}_1|\,|\vec{p}_3|}.$$

$\vec{p}_1, \vec{p}_2, \vec{p}_3$ stand for $\vec{p}_{t,p}, \vec{p}_{t,n}, \vec{p}_{t,d}$ and m is the proton mass. Here, Ω is the region in $\vec{p_1}$ space over which the integral is performed, and is determined by the Θ function. In the limit $q_{cut} \to 0$, we can replace $d\phi$ with $q_{cut}/(p_1/2)$ and $p_1 \to p_3/2$ to give

$$\rho(\vec{p}_3) \sim \frac{p_3}{2}\frac{2q_{cut}}{p_3} \exp(-\sqrt{\frac{p_3^2}{4} + m^2}/T_0) \exp(-\sqrt{\frac{p_3^2}{4} + m^2}/T_0) \tag{C.4}$$

$$\sim \exp(-\sqrt{p_3^2 + (2m)^2}/T_0) \tag{C.5}$$

If $q > 0$, the integration can be carried out numerically.

Bibliography

[Ahl93] L. Ahle, M.I.T., comparitive study of Auscon and Trck3 track reconstruction efficiencies.

[Bal93] T. Baltz and C. Dover at BNL are using $p_0 = 110\text{MeV/c}$, i.e. $q = 55\text{MeV/c}$.

[Bar86] J. Bartke, Phys. Lett. **B 174**(86) 32

[Bea89] D. Beavis *et al.*, Nucl. Inst. Meth. in Phys. Res. **A281** (89) 367

[Col92] B. Cole, *Particle Productioin at High Transverse Momentum in Nucleus-Nucleus Collisions at the AGS*, Ph. D. Thesis, Massachusetts Institute of Technology, (1992). (unpublished)

[Cos90] J. Costales, *Antiproton Production in Central Nucleus-Nucleus Collisions at 14.6 GeV/A*, Ph. D. Thesis, Massachusetts Institute of Technology (1990). (unpublished)

[Cse86] L. P. Csernai and J. I. Kapusta, Phys. Rep.**131**(86) 223

[Dup88] P. Dupieux *et al.*, Phys. Lett. **B 200**(88) 17

[Gol60] G. Goldhaber *et al.*, Phys. Rep.**120**(60) 300

[Gon91] W. G. Gong *et al.*, Phys. Rev. **C 43**(91) 781

[Gon92] M. Gonin, presented at the 7th Meeting of the APS **Division of Particles and Fields**, Nov. 10-14, 1992 Fermilab, IL

[Han90] O. Hansen, talk given at Summer School on Nuclear Physics, Mikolajki, Poland, Aug. 25 – Sept. 5, 1990

[Jac75] J. D. Jackson, *Classical Electrodynamics*, John Wiley & Sons, 1975

[Kop77] G. I. Kopylov, Phys. Lett. **50B**(74) 472

[Kun93] G. J. Kunde *et al.*, Phys. Rev. Lett. **70**(93) 2545

[Leo87] W. Leo *Techniques for Nuclear and Particle Physics Experiments*, Springer-Verlag, 1987

[Mek77] A. Mekjian, Phys. Rev. Lett. **38**(77) 640

[Mek78] A. Z. Mekjian, Nucl. Phys. **A312** (78) 491

[Mor90] R. Morse, *Bose-Einstein Correlation Measurements*, Ph. D. Thesis, Massachusetts Institute of Technology, (1990). (unpublished)

[Mos93] B. Moskowitz, presented at MIT-HIPAGS Jan 13-15, 1993

[NIM90] T. Abbott *et al.*, Nucl. Inst. Meth. in Phys. Res. **A290** (90) 41

[Pan92] Y. Pang, T. J. Schlagel, S. H. Kahana, Phys. Rev. Lett.**68** (92) 2743

[Pra84] S. Pratt, Phys. Rev. Lett. **53**(84) 1219

[Pra87] S. Pratt, M. B. Tsang Phys. Rev. **C 36**(87) 2390

[Pra92] S. Pratt, Fortran code that calculates the correlation function.

[Rol93] G. Roland, Private Communication, 1993

[RV93] V. Cianciolo and R. Soltz, Private Communication, 1993

[Sar89] M. Sarabura *Cluster Production in Relativistic Heavy Ion Collisions*, Ph. D. Thesis, Massachusetts Institute of Technology, (1989). (unpublished)

[Sch93] T. Schlagel, talk given at M.I.T.

[Vut92] V. Vutsadakis, *Small Relative Momentum Proton Correlations in Relativistic Heavy Ion Collisions*, Ph. D. Thesis, Massachusetts Institute of Technology, (1992). (unpublished)

[Won90] S. Wong, *Introductory Nuclear Physics*, Prentice Hall, 1990

[Zaj88] W. Zajc, in *Hadronic Multiparticle Production*, P. Carruthers, ed. (World Scientific Publishing Co., Singapore, 1988)

Acknowledgements

My first and foremost gratitude is reserved for Steve Steadman, who provided the intellectual environment in which I could work and grow as a scientist. It was a privilege to work so closely with him during the years I've been with the group. Despite his unbelievable workload, he often went out of his way to offer me guidance and advice. It would be difficult to thank him enough for all that he's done on my behalf.

George Stephans impressed me with his patience and insight, which incidentally makes him such a good listener. He always took the time to understand what I had to say, even when I was not being very clear about it. I found the conversations with him rewarding and beneficial. Oftentimes, I found the solution in the midst of describing the problem to him, for he has the amazing talent of asking the most poignant questions.

Though one can go on relying on the "kindness of strangers", as Blanche does, it's the familiar faces that you often turn to for assistance. This work would have never born my signature on it without the direct and the indirect helps I have received over the years from so many people around me. Ted S. and Vince C. taught me the most about the experiment and it would be hard to imagine myself trying to write this thesis without the knowledge I have gained through them. Ron S. also helped me on numerous occasions, including the time when I was studying for the General exams. In Pete R. and Larry A. I have found two more men I can rely on when help is needed, and Dave W. has been most helpful whenever I was having technical difficulties. I also had several interesting discussions with Dave M., Dan Z., and George H. My gratitude also extends to other members of the collaboration who worked hard to make the experiment a sucess. This thesis would not have been possible without their contributions.

I have much to learn from Craig Ogilvie, whose meticulousness in thinking often served to remind me what physics is all about. And it was a pleasure to know other new members of the group: Gunther R., Mark B., and Eleanor J. Though now they have left the group, Chuck P. and Brian C. were wonderful teachers, who endured my uninformed questions most patiently. Vassili V. has been a good friend every since we first met in the elevator. I always found his openness and optimism refreshing. Thanks to Walter K. who gave me a lift several times, when the group got together. The same goes for Vince, Ron, and Dave M.

Marge Neal brought my attention to the people and the world I had largely ignored out of convenience. In so doing, I believe, she has made me a better human being. And I appreciate Joanne S. and Barb C. for being so organized for all of us. The supportive assistance provided by the L.N.S. personnels is also sincerely acknowledged.

Finally, I thank E. Roth who introduced me to the worlds of art and music.